Experiments on a Flat Square Plate At high Angles of Attack

by

Muhammad Khaldoun Abdul-Gader Abu-Saleh

A Thesis Presented to the

FACULTY OF THE COLLEGE OF GRADUATE STUDIES

KING FAHD UNIVERSITY OF PETROLEUM & MINERALS

DHAHRAN, SAUDI ARABIA

In Partial Fulfillment of the
Requirements for the Degree of

MASTER OF SCIENCE

In

MECHANICAL ENGINEERING

July, 1987

Order Number 1360406

Experiments on a flat square plate at high angles of attack

Abu-Saleh, Muhammad Khaldoun Abdul-Gader, M.S.

King Fahd University of Petroleum and Minerals (Saudi Arabia), 1987

U·M·I
300 N. Zeeb Rd.
Ann Arbor, MI 48106

EXPERIMENTS ON A FLAT SQUARE PLATE AT HIGH ANGLES OF ATTACK

BY

MUHAMMAD KHALDOUN ABDUL-GADER ABU-SALEH

A THESIS PRESENTED TO THE
FACULTY OF THE GRADUATE SCHOOL
KING FAHD UNIVERSITY OF PETROLEUM & MINERALS
DHAHRAN, SAUDI ARABIA

IN PARTIAL FULFILLMENT OF THE
REQUIREMENTS FOR THE DEGREE OF

MASTER OF SCIENCE IN MECHANICAL ENGINEERING

JULY, 1987

بِسْمِ اللَّهِ الرَّحْمَٰنِ الرَّحِيمِ

KING FAHD UNIVERSITY OF PETROLEUM AND MINERALS

DHAHRAN, SAUDI ARABIA

This thesis, written by

MUHAMMAD KHALDOUN ABDUL-GADER ABU-SALEH

under the direction of his thesis committee, and approved by all the members, has been presented to and accepted by the Dean, College of Graduate Studies, in partial fulfillment of the requirements for the degree of

MASTER OF SCIENCE IN MECHANICAL ENGINEERING

Dr. Abdullah S. Al-Zakri
Dean, College of Graduate Studies

Date: July 25, 1987

Department Chairman
(Dr. Habib Abualhamayel)

Thesis Committee

Chairman (Dr. Muhammad U. Budair)

Member (Dr. Ing. W.H. Stahl

Member (Dr. Ing. Ronald Stuff)

ملخص البحث

ان ظواهر الجريان حول الصفائح المستوية ذات نسب الطول الى العرض المنخفضة لم تزل محاطة ببعض الغموض بالرغم من التطبيقات العملية المختلفة لتلك الصفائح مثل سطوح الرفع في الصواريخ والطائرات وفي أشباه الصفائح المستوية مثل المجمعات الشمسية واللاقطات الهوائية ودفات التوجيه في السفن. ويعتبر الانخفاض المفاجئ في قوة الرفع العمودية المؤثرة على مثل هذه الصفائح والمصاحب بتغيرات ظاهرة في سمات الجريان في جريان غير قابل للانضغاط عند زاوية عالية للتصادم أحد أهم هذه المظاهر . ويهدف هذا البحث الى دراسة أثر تغير رقم رينولد على سلوك الجريان حول صفيحة مستوية مربعه حادة الأطراف وعلى قوة الرفع العمودية المؤثرة على مثل تلك الصفيحة. ويشمل هذا البحث التجريبي على تجربة اظهار نمط الجريان وقياس متوسط الضغوط على سطحي الصفيحة وكذلك متوسط السرع في المستوي المركزي للصفيحة . وقد تم اجراء التجارب عند رقم رينولد يتراوح بين ٥ر٠ × ١٠^{٥} و ٣ر٧ × ١٠^{٥} وكذلك عند زوايا للتصادم تتراوح بين ٢٠° و ٥٠° . وبينت النتائج أن معامل قوة الرفع العمودية يتأثر بصعوبة مع تغيرات رقم رينولد عند ثبوت زاوية التصادم .كما أظهرت النتائج أن تأثير تغيرات رقم رينولد على نسبة الانخفاض في معامل قوة الرفع العمودية محسوسة عندما يتغير رقم رينولد بين ٥ر٠ × ١٠^{٥} و ٥ر١ × ١٠^{٥} بينما في المجال بين ٥ر١ × ١٠^{٥} و ٣ر٧ × ١٠^{٥} فان هذا التأثير ينخفض بشكل ملموس . وقد أبدت النتائج أيضا أن التغير في رقم رينولد ليس له أي تأثير مهم على شكل حدود الجريان خلف الصفيحة ولكن هذه الحدود تتسع للأعلى عندما تتغير زاوية التصادم من الزاوية تحت الحرجة الى الزاوية فوق الحرجة عند ثبوت رقم رينولد .

ABSTRACT

The flow structure about flat plate of low-aspect ratio is still not well known although such plates have various practical applications, as lifting surfaces on missiles,tail surfaces on airplanes and flat plate like structure as heliostats, antennas and ships rudders. One of the most important phenomenon is that the normal force acting on such plates in an incompressible flow experiences an abrupt drop at some high angle of attack and this is accompanied by certain changes in the flow field. The objective of the present investigation is to study the effect of varying the Reynolds number on the flow behaviour over a square flat sharp-edge plate as well as on the normal force acting on such plate. This experimental investigation includes surface flow visualization, mean pressure measurements and mean velocity measurements. It is carried out at Reynolds number ranging between 0.5×10^5 and 3.7×10^5 and at angles of attack between 20° and 50°. The results showed that the normal force coefficient is hardly affected by the change in Reynolds number for the same angle of attack, however, the influence of varying the Reynolds number on the percentage drop in the normal force is quite considerable as Reynolds number ranges between 0.5×10^5 and 1.5×10^5 while in the range between 1.5×10^5 and 3.7×10^5 the influence is reduced quite significantly. It is shown also that the change in Reynolds number does not have any significant influence on the shapes of the wake boundaries, however, the wake widen up when the angle of attack is changed from subcritical value to supercritical value for the same Reynolds number.

DEDICATED

to my Parents and my Wife without their prayers this work would never have come to a fruitful conclusion.

ACKNOWLEDGEMENTS

All praise to Allah for He is truly the One and only source of all knowledge.

I wish to express my sincerest appreciation to my thesis advisor, Dr. Muhammad U. Budair, for his help and guidance through my research. It was indeed an honour and a pleasure to have worked with him. I owe a debt of gratitude, also to Mr. M. Mahmoud from the Mechanical Engineering Department for his help.

I am grateful to my Thesis Committee members, Dr.-Ing. W.H.Stahl and Dr.-Ing. Roland Stuff for their review and interest in this work.

Finally I would like to acknowledge the assistance provided by Mr. M.N.Elabdin and the King Fahd University of Petroleum & Minerals, during the course of my research.

TABLE OF CONTENTS

LIST OF TABLES

LIST OF FIGURES

NOMENCLATURE

A	..	A spect ratio = $\frac{b^2}{S} = \frac{b^2}{b \times c} = \frac{b}{c}$
b	..	span
C	..	chord length
Cn	..	normal force coefficient = $\frac{N}{S\ q_\infty}$
Cp	..	mean pressure coefficient = $\frac{P - P_\infty}{q_\infty}$
$\bar{C}p$	..	average mean pressure coefficient
n	..	frequency of oscillation of the wake structure
P	..	local pressure on plate
P_∞	..	free stream pressure
q_∞	..	free stream dynamic pressure
Re_C	..	Reynolds number based on chord = $\frac{U_\infty C}{V}$
s	..	semispan
S	..	plan form area of plate
St	..	Strouhal number = $\frac{nC}{U_\infty}$
u'_{rms}	..	root-mean-square of velocity fluctuation
U_∞	..	free stream velocity
U	..	local mean velocity
X	..	coordinate dimension coincide on the chord
X'	..	coordinate dimension parallel to free stream direction
Y	..	coordinate dimension coincide on the span
Z	..	coordinate dimension vertical to X-Y plane
Z'	..	coordinate dimension perpendicular to free stream direction

Greek symbols

α	..	angle of attack
α_{crit}	..	critical angle of attack
ν	..	kinematic viscosity
ρ	..	density.

1. Literature Survey and Statement of the Problem

It has been observed very early, that the normal force acting on a flat plate of low-aspect ratio as well as circular disc in an incompressible flow, experiences an abrupt drop at some high angle of attack, α, and that is accompanied by certain changes in the flow field. Such a sudden drop in the normal force has negative effects on the performance of such plate which has various practical applications, as lifting surfaces on missiles, flat plate like structures as in heliostates, antennas, and ships' rudders.

The interest in this phenomenon goes back to 1890 when W.H. Dines(7) noticed a sudden drop in the normal force acting on a square plate, when the angle of attack changed from 35° to 40°. Similar results were reported by L.Prandtl in 1910 (16), and S.F.Hoerner in 1965 (12). In order to get insight into the origin of drag, F. Ahlborn in 1904 (1) visualized the flow field about a thin rectangular flat plate in a water tank at angles of attack between 70° and 90° to the wind direction. He observed that a vortex ring is formed behind the plate. This vortex ring is more or

less symmetrical about the streamwise central plane at angle of attack 90^{o} and becomes asymmetrical when the angle of attack is less than 90^{o}. In 1905 in subseuqnet experiments on a square plate (2) at angle of attack of about 30^{o}, he observed that the original vortex ring ruptures at the trailing edge with two loose ends trailing down stream on either side. He related this to a sudden change in drag. In 1909 (3) he tested also rectangular plates of aspect ratios A=2 and A=3. He found that a closed vortex ring existed on the rear of the plates at high angles of attack between 45^{o} and 90^{o} and this closed vortex ring changed to a M-shaped vortex with trailing vortices near side edges at angles of attack betwen 25^{o} and 45^{o} ,see Fig.(1.1).

In 1912 C.G. Eden (8) investigated water flow over a rectangular plate extending over the entire test section at different angles of attack between 0^{o} and 90^{o} to the flow direction and at Reynolds number, based on plate chord of $Re_{c}=1.9x10^{5}$. He found that at small angles of attack up to 9^{o} no eddies were formed. The formation of eddies along with "dead water" region at the back of the plate were clearly shown at an angle of attack of about 10^{o}. In a comparative study he demonstrated the similarity of flow in air and

water. He used a wind channel of 15.2x15.2 cm in cross-section in which eddies could be shown by means of smoke. He photographed the eddies in the two media. Figs.(1.2) and (1.3) show the type of flow which prevails at low velocities, and Figs.(1.4), (1.5), (1.6),and (1.7), show the periodic eddies which are formed when the velocity is increased. The change from the first type to second type was seen to occur in water and air when vl^*/ν reached a certain value which was approximately the same in each medium.

A. Fage and F.C. Johansen in 1927 (9) studied the flow behind an infinitely long thin flat sharp-edged rectangular plate at different angles of attack and at Reynolds number $Re_c=2.2x10^5$. They measured the normal force distribution as well as the dimensions and the strength of the individual varticies observed behind the plates. They showed that the vortices generated at each edge pass down stream with a frequency that increases as the angle of attack decreases while it is proportional to the wind speed at constant angle of attack. The result showed also that the vortices are shed from the two edges of the plate at the same rate. This rate falls down as the angle of attack gets less than 90^o. Later, in (11) an account was given of early investigations of the

three dimensional flow field behind bluff bodies and its development with Reynolds number. A creeping flow (Re<<1) past a normal plate remains attached to the rear side. With increasing Reynolds number the flow separates, and a region, separated from the main stream by a vortex sheet is formed behind the plate. Inside the region, a permanent vortex ring exists. Such a flow pattern was observed behind circular plates from Re =5 to Re =100-200 by T.E. stanbon and D. Marshall (21); L.F.G. Simmons and N.S. Dewey (19) in 1931. For higher Reynolds number, the vortex ring breakes down with successive portions of it carried downstream at some distinct frequency.

A number of rectangular flat sharp-edged plates of various aspect ratios were used by H.Winter in 1935 (24) to investigate the effect of aspect ratio on the abrupt change in normal force at critical angle of attack α_{crit}. He concluded that the magnitude of the drop in normal force decreases with increasing aspect ratio, and thus the change becomes smoother. His experiments were extended to high angles of attack, and showed that the normal force acting on a square flat plate drops abruptly by about 40% at angle of attack of about 40°. These experiments performed at Reynolds

number ranging between $Re_c=3x10^5$ and $1.7x10^6$.

In 1959 R. Fail, J.A. Lawford and R.C. Eyre (10) conducted experiments on flat plates placed perpendicular to the wind direction at speed of about 43 m/s. They studied the effects of aspect ratio of flat plates on the flow pattern, drag, and surface pressure. They concluded that as the aspect ratio is increased from unity, the drag coefficient rises, the base pressure falls and the bubble length decreases. These changes are relatively small up to an aspect ratio of 10, thereafter the changes are more rapid. Later in 1965 S.F.Hoerner (12) showed that the normal force coefficient for an inclined disc remains almost constant at 1.17 over a range of angle of attack between 45 and 90 and is equal to that of an inclined square plate, see Fig.(1.8). J.R. Calvert in 1967 (6) studied the periodic changes occuring in the wakes and visualized the flow behind a circular disc and square plates for angles beyond α_{crit} and $Re_c=4x10^5$. He noticed that at angle of attack of more than 20^o a strong vortex shedding was visible and th flow pattern behind the disc is similar to that behind a square plate photographed by C.G.Eden (8). He observed also, that as the angle of attack is increased, the

vortex shedding becomes more regular.

L.Robert in 1979 (17) studied the effect of Reynolds number on the aerodynamic characteristics of a body with cruciform wings at angles of attack up to 50^{o}. Both pressure distribution and force balance tests were made at Reynolds numbers based on body diameter from approximately $Re_c=1.3x10^5$ to $28x10^5$, and roll angles 0^{o}, 22.5^{o}, and 45^{o}. He concluded that force and moment coefficients consisting of normal force, side force, pitching moment, yawing moment, and rolling moment were found to be essentially independent of Reynolds number for complete range of test conditions. He also found that there is no significant Reynolds number effect on prssure coefficient distribution in the wind ward wing-body interaction region.

A.E. Winkelman and J.B. Barlow (25) in 1979 conducted tests using a series of rectangular plan-form wings all with the same 8.29 cm chord at different aspect ratios. The tests were carried out at Reynolds number ranging between $Re_c=2.45x10^5$ and $3.85x10^5$. They propose a new general flowfield model for the separated flow over a rectangular plan-form wing at subsonic speeds and high angles of attack.

They found that a mushroom-shaped three-dimensional separation cell started to develop at angle of attack $\alpha=10^{o}$. The first signs of trailing edge separation occured at $\alpha=15^{o}$. The trailing edge stall-cell grew in size till $\alpha=26.1^{o}$, then, the surface pattern abruptly changed and the three-dimensional separation line extended to the leading edge. This abrupt change was accompanied by a sudden loss of lift and a noticeable increase in wing buffeting. With increasing α, the counter-rotating swirl patterns were located near the wing tips and uniformly reversed surface flow existed over most of the span.

In 1980 J.H. Strickland (18) studied vortex shedding from square plates, placed normal to a ground plane, simulating wind effect on solar collectors which can be approximated as square plates near the ground plane. It was shown that the strouhal number decreases with Reynolds number especially between $Re_c=1.4x10^4$ and $1.5x10^5$. The strouhal number is defined in this case as

$$S = n.c\ /U_\infty$$

where n is the frequency of oscillation of the wake structure, U_∞ is the free stream velocity, and c is the

chord of the plate. Satya Pal. in 1981 (20) studied the effect of free stream turbulence on the characteristics of a turbulent wake developed from the trailing edge of a flat plate at angles of attack -3°, 0°, and 6°. He concluded that the mean velocity profiles are observed to be asymmetrical about the wake center line when the wake is influenced by the pressure gradient and free stream turbulence. The similarity in the mean velocity profile is maintained to a good extent when the profiles are normalized with respect to the turbulence parameters.

Recently W.H. Stahl, and M.Mahmood in 1984 (22) studied the flow phenomenon associated with the abrupt loss in normal force at some high angles of attack. Their experiments were done on a flat square plate at $Re_c=1.1x10^5$ and carried out in the UPM low-speed wind tunnel. In this investigation particular attention was given to find the causes leading to the abrupt and considerable fall in the normal force with increasing the angle of attack. They concluded that the fall in the normal force acting on the square sharp-edged plate is accompanied by sudden disappearing of the tip vortices from the plate surface. They found that the amount of the normal force coefficient

loss is about 15% and it occured at an angle of attack of about 30^{o}.

After considering W.H. Stahl and M.Mahmood study and the relevant information available in the literature it was felt that the study of the effect of Reynolds number on the variation of the normal force would be a desirable objective of the present study.

2. Experimental Procedure

2.1: Introduction:

The original motivation for this study developed out of an investigation previously done by W.H. Stall and M. Mahmood (22). Their investigation was done in the UPM low-speed wind tunnel at Reynolds number $1.1x10^5$. They studied the phenomenon of abrupt and large changes in normal force occuring at some high angle of attack and constant Reynolds number, on a square flat sharp-edged plate. Therefore, the scope of present investigation was to study the effect of varying Reynolds number on the abrupt changes in the normal force along with the flow behavior on the square flat sharp-edged plate and its wake. The work was carried out at Reynolds number ranging between $Re_c=0.5x10^5$ and $Re_c=3.7x10^5$ and at angles of attack between $\alpha=20^o$ and $\alpha=50^o$. It was done using the same models and same experimental set-up designed by W.H. Stahl and M. Mahmood and involved essentially the folowing experiments:

a)- Surface flow visualization.

b)- Mean Pressure measurements.

c)- Hot-wire measurements.

2.2: Wind tunnel:

The experiments were carried out in the low-speed wind tunnel of KFUPM Aerodynamic Laboratory. It has a closed test section of rectangular shape with dimensions of 1.1x0.8 m and a length of 3.5 m. The tunnel is of the open-return type, with a maximum wind speed in the empty test section of about 35 m/s. Fig.(2.1) shows the Wind Tunnel in position. The speeds at which the wind tunnel ran and the corresponding Reynolds numbers are as listed in table (2.2.1).

2.3: Models and Mounting Arrangements:

As was mentioned earlier, the experimental set-up and models designed by W.H. Stahl and M. Mahmood in their work on flat plate (22) have been utilized in the present investigation.

The models are two flat sharp-edged square plates of 22 cm chord length and made of plxiglass. One was used for flow visualization and the other for pressure measurements. The model used for flow visualization has a thickness of about 4% of the chord and chamfered edges kept at an angle

of about 15^{o}. The pressure model was provided with 144 holes of diameter 0.8 mm spaced on one surface of the plate according to Fig.(2.2). It has a thickness of about 7% of the chord with chamfered edges kept at an angle of about 16^{o}. The pressure holes were connected to the pressure manometer one by one by polythelene tubes in order to measure the mean pressure on the plate surface Figs.(2.3) and (2.4) show the models used for flow visualization and mean pressure measurements respectively.

The support designed to hold the model in position is shown in Fig.(2.5). A hinge was provided between the horizontal pipe of the fixture and the sting fixed to the plate to allow changes of angle of attack. Vibrations of the model were reduced by bracing the horizontal pipe with three wires. Care has been taken to make the parts facing the wind well streamlined. The connecting tubes to the outside manometer were arranged around the support in such a way as to provide as little interference as possible. The models could be oriented in the free stream between $\alpha=0^{o}$ and 90^{o}.

2.4: Flow Visualization Procedure and Equipments:

The patterns of the flow along the surface of the plate were made visible by means of the surface oil-flow technique. A mixture of kerosene and chalk powder were sprayed evenly over the plate surface by means of a spray gun and then the model was exposed to the wind. This technique helps to observe the changes in the flow patterns at different angles of attack, especially the changes due to varying the angle of attack before and after the critical angle α_{crit}. The flow patterns were visualized on the suction and pressure sides of the plate at angles of attack between $\alpha = 20^{o}$ and $\alpha = 50^{o}$. This method revealed the direction of surface streamlines and helped to determine α_{crit} for each Reynolds number considered, refer to table (2.2.1). Air compressor was used to provid pressurised air to spray the kerosene and chalk powder mixture over the surface of the model.

2.5: Mean Pressure Measurements Procedure and Equipments:

Mean pressures were measured on suction and pressure sides of the plate, especially near the critical angle of attack. The purpose of pressure measurements was to study the effect of Reynolds number on the abrupt change in the

normal force acting on square flat plate as well as the pressure distribution over the two sides of the plate at different angles of attack and different Reynolds numbers.

As described in section 2.3, the pressure model was machined in UPM workshops from plexiglass. It was a square flat sharp-edged plate with 22 cm chord and thickness of about 7% of the chord. The edges were chamfered and kept at angle of about 16^{o}. It has 144 holes of diameter 0.8 mm distributed over one surface of the plate. Mean pressures on suction and pressure surfaces could be measured at the same holes by rotating the plate through 180^{o} ;thus, the surface facing the wind is no longer chamfered but flat, so that the pressures on the suction side may be slightly different but no attempt has been made to correct for this effect.

The mean pressures were measured at four different Reynolds numbers listed in table (2.2.1), by means of water manometers of the projection type along with a pitot static tube fixed to the top surface of the test section. Fig.(2.6) shows the manometer in operation. The values of the normal force coefficients, Cn , were estimated from the mean

pressure coefficients $(P-P_\infty)/0.5\rho U^2_\infty$ measured on suction and pressure sides of the plate.

2.6: Velocity Measurements Procedure and Equipments:

2.6.1: Hot-wire and Measurements Set-up:

One hot-wire probe was used for this investigation in order to measure the magnitude of the mean velocity and the root-mear-square (rms) values. The probe sensor was of the type Disa 55P11 that consists of 5 μm-diameter platinum-plated tungesten wire of length of about 2 mm. The hot-wire was connected to a constant temperature anemometer of the type Disa 55M10. The output signal from the anemometer was fed to a linearizer of the type Disa 55M25. The magnitude of the mean velocity and the rms values could be measured by means of digital voltmeter of the type Disa 55M31 and RMS Unit of the type Disa 55D35 respectively Fig.(2.7). The hot-wire was calibrated by the calibration equipment of the type Disa 55D90 which consists of 55D44 Pressure control unit, 55D45 nozzel unit and 55D46 pressure converter unit Figs.(2.8) and (2.9).

A 3-D coordinate system was chosen such that the origin

was located at the leading edge and the center line of the plate was at y=0, see Fig.(2.10). The hot-wire measurements were taken in the x-y plane of the Fig.(2.10). For each x station the hot-wire was moved vertically upward and downward along a line parallel to the Z'-axis. The hot-wire was supported by means of probe support which was attached to a traversing mechanism mounted in the test section as shown in Fig.(2.11).

2.6.2: Velocity Field Measurements:

The measurements of the mean velocity and root-mean-square profiles took place on the suction side of the plate in the central plane at y=0, see Fig.(2.10). The measurements covered about 2 times the chord length from the leading edge along the wind direction x' and about 1.5 times vertically to the wind direction Z'. The measurements along the Z'-axis extended about 82% of the chord fromd the leading edge along the positive Z'- axis and about 68% along the negative axis. The step movement was 1 cm in both x' and Z' directions. Fig.(2.12) shows the stations at which the mean velocity and root-mean-square profiles were measured.

The mean velocity measurements and root-mean-square values were taken at two different Reynolds numbers which are $Re_c=0.5x10^5$ and $Re_c= 1.5x10^5$. At each Reynolds number two angles of attack were chosen one is subcritical $\alpha=25^o$ and the other is supercritical $\alpha=32^o$ between which the normal force changes abruptly. These measurements were mainly used to determine the mean boundaries of the wake at the central plane. The mean boundary of the wake was determined basd on the definition that the edge of the wake occurs at the point where a maximum mean speed is obtained (9).

3. Results and Discussion

3.1: Introduction:

In this chapter, results of the outlined experimental steps in chapter 2 are discussed, starting by the surface flow visualization which is used to obtain the flow patterns and the changes that take place on the plate surface due to the effect of varying Reynolds number and angle of attack. The discussion also includes the mean pressures measured on the surfaces of the plate at different Reynolds numbers and different angles of attack to determine the effect of Reynolds number on the abrupt change in the normal force and on the pressure distribution over the surfaces of the plate. Finally, the discussion is concluded by examining the velocity profiles and the central wake boundaries measured by meanse of hot-wire at two different Reynolds numbers, $Re_c=0.5x10^5$ and $1.5x10^5$, and for two angles of attack, $\alpha=25^o$ and $\alpha=32^o$.

3.2: Flow Visualization:

The flow visualization experiment was carried out by

means of the surface oil-flow technique to observe the changes in the flow pattern on the flat plate at different angles of attack and different Reynolds numbers. In this method the plate surface was spread over with a mixture of kerosene and chalk powder by using spray gun. When the flow is set up the mixture of kerosene and chalk powder follows the flow pattern on the plate surface. This technique was found to be very useful at a relatively high Reynolds numbers and could not give reliable results at lower Reynolds numbers.

It was observed that the flow pattern on the suction side of the plate changed between $\alpha=28^{o}$ and $\alpha=32^{o}$ for all Reynolds numbers considered except for $Re_c=0.5x10^5$ where this technique did not work well. It was easy to distinguish between the flow patterns obtained for $\alpha<28^{o}$ and $\alpha>32^{o}$. This was clearly observed for all Reynolds numbers in question except for Reynolds numbers below $Re_c=1.5x10^5$ where it was difficult to clearly make the flow pattern visible because of the apperantly weak forces acting on the plate , see Figs.(3.1),(3.2),(3.3), and (3.4).

The critical angle of attack α_{crit} was observed to be

about 30^{o} for all the Reynolds numbers considered. Actually this is the angle around which the normal force changes abruptly as the calculation of such force indicates from the pressure distribution over the two faces of the plate. This is reflected by the flow patterns shown in Figs. (3.1), (3.2), (3.3), (3.4), and (3.6). The behaviour of the flow is thus clasified into two regimes, the subcritical and the supercritical.

3.2.1: Subcritical Regime :

For the case of flow at subcritical incidences, i.e., $\alpha<30^{o}$ the flow pattern on the suction side was characterized by a formation of two eyes (Foci) denoted by (F), a node of attachment (N) and a saddle point (S), see Fig.(3.7).

As it could be seen in Figs.(3.1) and (3.2) the air flows over the suction side of the plate and seems to reattache at some node (N) near the trailing edge at which the streamlines spread almost in all directions. Also, a highly three-dimensional separation line extending to both sides of the plate from (S) towards the two Foci (F) is obsrved and seems to move towards the leading edge as Reynolds number is increased for the same angle of attack. In addition, it is

clear that the streamlines coming from the leading edge meet at the separation zone with those coming from the node towards the leading edge.Furthermore, it is observed that as the Reynolds number increases the flow pattern and the eyes on the suction side get more visible .

The flow pattern for $\alpha < 30$ as revealed in the present investigation showed similar behaviour to that given by Winkelman (25) for rectangular plate of aspect ratio 3.5 at $\alpha=22.8^{o}$ and $Re_{c}=2.45x10^{5}$ as indicated by Fig.(3.8). Also, the surface flow patterns obtained for subcritical and supercritical regimes were similar to those observed by W.H.Stahl and M.Mahmood(22) .

3.2.2: Supercritical Regime :

For the case of flow at supercritical incidences,i.e., $\alpha>30^{o}$,the surface flow pattern on the suction side indicated clearly a separation near the leading edge as shown in Figs.(3.3) and (3.4). It is noticed that as the Reynolds number icreases the separation line near the leading edge gets to be closer to that of two-dimensional separation line. Also one obvious feature in this range is the disappearing of the two Foci(F) for all Reynolds numbers

where the flow could be made visible. It is also observed that for both regimes the separation line moves towards the leading edge as Reynolds number is increased.

As could be seen in Fig.(3.5) the surface flow visualization on the pressure side of the plate indicates flow attachment near the leading edge and the flow pattern did not show any significant changes with the increase in Reynolds number and angle of attack for both subcritical and supercritical ranges that were invistigated.

3.3: Pressure Measurements:

Mean pressure measurements were carried out on the suction and pressure sides of the plate at different angles of attack and different Reynolds numbers to study the influence of Reynolds number on the normal force experienced by the flat square plate at different angles of attack and to get an insight into the flow phenomenon on both sides of the plate. The average mean pressure coefficients Cp and the normal force coefficients Cn on the plate surfaces were estimated by means of pressure distribution on both sides of the plate. The estimated values of Cp and Cn are given in table (3.3.1).

3.3.1: Subcritical Regime :

3.3.1.1: Suction Side :

Figs.(3.9),(3.10) and (3.11) show the chordwise pressre ditribution over the suction side of the plate for the angles of attack $\alpha=25^{o}$, 28^{o} and 29^{o} and for all the Reynolds numbers considred.It is evident from Figs.(3.9) and (3.10) that for all Reynolds numbers in question the suction level increases gradually till maximum suction is achieved at a distance of about 40% of the chord length measured from the leading edge for $Re_{c}=3.7x\ 10^{5}$. The maximum suction tends to move towards the trailing edge as the Reynolds number is decreased. This conforms with the observation that the separation line tends to move towards the leading edge as Reynolds number is increased, Figs.(3.1) and (3.2). After the maximum suction is acheived for all Reynolds numbers it starts to decrease continuously till the trailing edge of the plate . This implies that the pressure on the suction side of the plate decreases chordwise till minimum is attained then starts to build up till the region designated as a node (N). This conforms with the flow pattern suggested by the surface flow visualization in which

the stream lines coming from the leading edge and those coming from the node meet at the separation zone, refer to Figs.(3.1) and (3.2). As could be seen from Fig.(3.11), for $\alpha = 29^{o}$, the suction achieves maximum at about 40% of the chord measured from the leading edge at y/s= 0.00 and 0.27 while at y/s=0.54 , 0.81 and 0.89 the maximum is attained at about 50% of the chord length. This littel differnce between the pressure distribution behaviour at $\alpha=29^{o}$ and that at $\alpha=25^{o}$ and 28^{o} is thought to be due to the fact that the angle of attack $\alpha=29^{o}$ is very close to the critical angle and so the flow behaviour over the plate may supercritical at sometimes or totaly subcritical at othertimes.This actually was observed during taking pressure measurments at this angle.

Fig.(3.18) shows the spanwise pressure distribution for the angle of attack $\alpha=28^{o}$ over the suction side of the plate and for all the Reynolds numbers cosidered. It is observed here that closer to the trailing edge, at x/c=0.945 and 0.82, the pressure on the suction side of the plate decreases spanwise more sharply beyond 20% of the semi-span measured from the center of the plate. At x/c=0.59 ,the pressure decreses and gets to a minimum around 70% of the

semi-span and then starts to increase. Furthermore towards the leading edge, at x/c=0.41 ,the minimum pressure is attained at about 30% of the semi-span. At x/c=0.182 and 0.054 the pressure achieves minimum at about 55% of the semi-span. All of this indicates that if there is a separation it will occur between x/c=0.59 and 0.054 . This also conforms with the surface flow visualization results shown in Figs.(3.1) and (3.2).

Fig.(3.23) shows the average mean pressure coefficient vs. Reynolds number on the suction side of the plate. It is observed that the amount of suction as reflected by the mean pressure coefficient is not influenced by the increase in Reynolds number when the angle of attack is fixed. However, the suction is increased as the angle of attck is increased when the Reynolds number is fixed as evident from Fig.(3.27).

3.3.1.2: Pressure Side :

Figs.(3.12) and (3.13) show the chordwise pressure ditribution over the pressure side of the plate for the angles of attack $\alpha=25^{o}$ and 28^{o} and for all Reynolds numbers considered. The spanwise pressure distribution for $\alpha=28^{o}$ is

shown in Fig.(3.19). It is observed that for all Reynolds numbers in question the static pressure on the pressure side of the plate decreases smoothly chordwise and spanwise over most of the plate as evident from Figs.(3.12),(3.13) and (3.19). This decrease in pressure in both direction, spanwise and chordwise , conforms with the surface flow visualization results shown in Fig.(3.5). As could be seen from Fig.(3.24) which represent the average mean pressure coefficient on the pressure side of the plate vs. Reynolds number, the average mean pressure coefficient dose not change much as Reynolds number increases for the same angle of attck while a slight change occurs when the angle of attack is increased from $\alpha=25^{o}$ to 28^{o}.

It has been seen from above discussion that for subcritical regime the average mean pressre coefficient on both suction and pressure sides of the plate does not change much as Reynolds number is increased for the same angle of attack, however,it increases as angle of attck is increased as shown in Fig.(3.27). This indicates that for subcritical regime the normal force coefficient dose not vary appreciably with the increase in Reynolds number as evident from Fig.(3.25) and increase with angle of attack as shown

in Fig.(3.28).

3.3.2: Supercritical Regime :

3.3.2.1: Suction Side :

Figs.(3.14) and (3.15) show the chordwise pressure distribution over the suction side of the plate for the angles of attack $\alpha=32^{o}$ and 35^{o} and for all Reynolds numbers considered. It is observed here that the suction level does not change much with the increase in Reynolds number and the pressure distribution is almost constant over the entire plate at all Reynolds numbers in question. It is also observed that as the angle of attack increases from $\alpha=32^{o}$ to 35^{o} the pressure distribution curves for all Reynolds numbers cosidered seem to coincide on each other which means that the difference in suction in chordwise direction is negligible as Reynolds number is increased. The suction level , however , dropps cosiderably as compared to the subcritical regime as clearly shown in Fig.(3.22). Fig.(3.20) shows the spanwise pressure distributin for the angle of attack $\alpha=32^{o}$ over the suction side and for all Reynolds numbers cosidered . It is obvious here that the suction between x/c= 0.054 and x/c= 0.59 looks to be leveled

while at x/c= 0.82 and 0.904 starts to increase spanwise. This conforms with the surface flow visualization results shown in Figs.(3.3) and (3.4). It is evident from Fig.(3.23) that for the supercritical regime the suction is hardly affected by the increase in Reynolds number. However, it is varied with angle of attack as shown in Fig.(3.27).

3.3.2.2: Pressure Side :

Figs.(3.16) and (3.17) show the chordwise pressure distribution over the pressure side of the plate for the angles of attack $\alpha=32^{o}$ and 40^{o} and for all Reynolds numbers considered.It is observed here that the pressure decreases smoothly chordwise. However, the pressure curves seem to get more leveled over most of the span except at the side edge where the drop in pressure is more pronounced as could be seen from Fig.(3.21). The spanwise and chordwise pressure variation, on the pressure side for the supercritical regime look similar to those for the subcritical regime. This is supported by the surface flow visualization results shown in Fig.(3.5). It is interesting to notice that at $\alpha=40^{o}$ the chordwise pressure distribution curves seem to collapse on each other which may reflect the insignificant effect of the

Reynolds number at such angle of attack. This explains the tendency of the average pressure coefficient curve for $Re_c=0.5x10^5$ at $\alpha=40^o$ in Fig.(3.27). It is also observed from Fig.(3.24) that for supercritical regime the average pressure coefficient is negligibly afected by the icrease in Reynolds number for the same angle of attack .

It may be suggested from the above dicussion that for the supercritical regime the average pressure coefficient on both sides of the plate is not influenced significantly by the variation in Reynolds number if the angle of attack is fixed as shown in Figs.(3.23) and (3.24). However the influence of Reynolds number variation is more pronounced as the angle of attack is varied as evident from Fig.(3.27). This leads to the observation that for the supercritical regime the normal force coefficient does not vary cosiderably with Reynolds number if the angle of attack is kept the same as shown in Fig.(3.25) while it is more influenced by the variation in angle of attack at the same Reynolds number, Fig.(3.28).

Fig.(3.28) shows the variation of the normal force coefficient Cn with the angle of attack α. The present

results show that for all Reynolds numbers considered the same typical abrupt drop in the normal force is observed at the critical angle of attack as was previously observed by H.Winter (24) and W.H.Stahl and M.Mahmood (22). In the present investigation, however, the relative drop in Cn values for all Reynolds numbers investigated is less than that reported by H. Winter (24) for flat square plate at Reynolds number ranging between $Re_c=3.0x\ 10^5$ to $1.7x\ 10^6$.

Fig.(3.26) shows the variation of the percentage drop in the normal force coefficient ΔCn% with the Reynolds number. The estimated values of ΔCn% are calculated between $\alpha=28^o$ and 32^o and given in table (3.3.2). It is observed that the ΔCn% is linearly increased from 8.6 to 17.9 as Reynolds number is increased from $0.5x10^5$ to $1.5x10^5$ then gradually acheives the value of 19.5 at $Re_c=2.6x10^5$. As Reynolds number is increased to $3.7x10^5$ the ΔCn% gets a value of 18.4. This may be suggested that the influence of Reynolds number on the percentage drop in the normal force coefficient is quite significant as Reynolds number ranges

between $0.5x10^5$ and $1.5x10^5$. However, the influence of Reynolds number on $\Delta Cn\%$ is reduced quite significantly in the Reynolds number range between $1.5x10^5$ and $3.7x10^5$ as it may be observed in Fig.(3.26).

3.4: Velocity Field:

3.4.1: Introduction :

The hot-wire probe was placed parallel to the span of the plate. Consequently, the magnitude of the mean velocity values measured by the hot-wire indicates the velocity vector in the plane normal to the span of the plate. The reliablity of the hot-wire signal at any station was determined by measuring the root-mean-squre value of the velocity fluctuation to the local mean velocity (u'_{rms}/U). At all stations the maximum mean velocity was located precisely by moving the hot-wire in a continuos manner until a maximum mean velocity was obtained. The central mean wake boundary was determined based on the difinition that the edge of the wake is obtained at a point where a maximum mean velocity occurs.

3.4.2: Subcritical Regime :

Fig.(3.29) shows the mean velocity pofiles on the suction side of the plate at the central plane and for $Re_c=0.5x10^5$ and $\alpha=25^o$. The horizontal axis corresponds to the local mean velocity normalized with respect to that of the free stream. Referring to the velocity profile at x/c=0.00, the closest data point to the tip of the plate is at Z'=5 mm and any attempt of positioning the probe closer to the plate was feared might damaged the probe. The magnitude of the normalized velocity at this location is about 0.974 and greater than the other values of the same profile. This value was taken as the maximum velocity in this profile. The reliability of the hot-wire signal at this point is about 4% and does not exceed this value as the probe is moved vertically away from the plate surface.

At x/c= 0.05 the maximum mean velocity occurs at Z'= 12 mm with u'_{rms}/U value of about 8% . The normalized velocity at this location is about 1.102.

The measurements at x/c=0.201 begins with the closest data point to the plate surface at Z'=-20 mm at which the normalized velocity is 0.222. At this location the reliability of the hot-wire signal is very poor since a

value of u'_{rms}/U was about 74%. The mean velocity profile starts with the maximum mean velocity that occurs at Z'=25 mm at which the u'_{rms}/U is about 8%.

Further down stream at x/c=0.351, the mean velocity values close to the plate surface show high u'_{rms}/U values, as for instance at Z'=-15, 5 and 15 mm, the root-mean-square fluctuation ranged between 71% and 91% . The maximum mean velocity was obtained at Z'=35 mm at which the ratio u'_{rms}/U is about 10% .

At x/c=0.552, the reliability of the hot-wire singals decreases as compared to those observed at x/c=0.351, however, the u'_{rms}/U value ranges between 59% at Z'=35 mm and 100% at Z'=-5 mm. The maximum mean velocity was obtained at Z'=33 mm at which the normalized velocity is about 1.136 and the ratio u'_{rms}/U is about 9%.

Similarly at x/c=0.752, the maximum mean velocity was located at Z'=25 mm at which the ratio u'_{rms}/U is about 8% and the normalized velocity is about 1.067.

At the trailing edge, at x/c=1.003, the maximum mean velocity occurs at Z'=15 mm at which the normalized velocity

is about 1.236. the reliability of the hot-wire signal is very poor as the probe is moved closer to the plate.

Very adjacent to the trainling edge, at x/c=1.053, it is observed that as the hot-wire probe is moved away from the trailing edge in either Z' direction, the signals of the probe become more reliable. However the hot-wire signal is not reliable in the vicinity of the trailing edge.This is the reason why the velocity profiles at this station and at, for instance, x/c=1.103, 1.154, 1.254 are broken into two parts as shown in Fig.(3.29).

The mean velocity profiles at x/c=1.304, 1.404, 1.505 and 1.605, are continuous curves. They show minimum values in the region behind the traling edge. At the maximum velocities the ratio u'_{rms}/U does not exceed 8%. The values of the normalized velocities at these stations are 1.134, 1.136, 1.158 and 1.174 respectively.

At further downstream stations like x/c=1.755, 1.906, and 2.106 it is observed that the mean velocity profiles show very little variation. As the hot-wire probe is moved further downstream, the signals showed high degree of reliability an indication that the probe was almost getting

outside the recirculation region. Also, the unreliable reading observed closer to the plate surface can be related to the fact that in such region there is recirculation in the flow in which case the hot-wire would not distinguish the direction of flow.

The mean velocity profiles on the suction side of the plate at the central plane were also measured for $Re_c=1.5x10^5$ and $\alpha=25^o$, see Fig.(3.30). It is observed from Fig.(3.29) that the the unbroken profiles start at x/c= 1.304 onward. This suggests that the high turbulent region extends up to about x/c= 1.304. The profiles for the case when the plate was at $\alpha=25^o$ and $Re_c=1.5x\ 10^5$ show that the high turbulent region extends up to about x/c= 1.404.

Fig.(3.33) shows the central mean wake boundary at $\alpha=25^o$ for the two Reynolds numbers cosidered. Each data point shown in this figure corresponds to the location where the maximum velocity occurs for each profile, see Figs.(3.29) and (3.30). It is observed here that for the subcritical regime the central mean wake boundary is insignificantly affected by the change in Reynolds number. This seems to cnoform with the remarks , made earliar , that the influence

of Reynolds number on the average mean pressure coefficient measured on the suction and pressure sides for the same angle of attack is negligible ,see Figs.(3.23) and (3.24).

3.4.3: Supercritical Regime :

Mean velocity profiles were measured at $\alpha=32^{o}$ for $Re_{c}=0.5x10^{5}$ and $1.5x10^{5}$ shown in Figs.(3.31) and (3.32). The velocity profiles in those regimes suggest that the high turbulent region is extended further downstream than the subcritical case.

Fig.(3.34) shows the central mean wake boundary for $\alpha=32^{o}$ at the two Reynolds number considered. It is observed that the boundaries are very much the same. This leads to the suggestion that the change in Reynolds number does not have a significant influence on the shapes of the wake boundaries. This again seems to conform with the notion made earlier that at the supercritical range the mean pressure coefficient on the suction and pressure sides of the plate is not influenced significantly with the change in Reynolds number.It is observed also that the wake widens up when the angle of attack is changed from the subcritical value ($\alpha=25^{o}$) to the supercritical value ($\alpha=32^{o}$) for the Reynolds

number. This is actually shown by comparing Figs.(3.33) and (3.34) which were drawn to scale.This agrees the flow visualization reported in (26).

4. Summary and Conclusion

An experimental investigation of the flow over a square flat plate was carried out in a low-speed wind tunnel at different Reynolds numbers and different angles of attack. This investigation included surface flow visualization, mean pressure measurements and mean velocity measurements. The flow visualization and mean pressure measurements were conducted on the suction and pressure sides of the plate. The mean velocity measurements were coducted in the central plane of the wake. The purpose of this investigation was to study the effect of varying the Reynolds number on the flow behaviour over the plate as well as on the normal force coefficient.

The surface flow visualization was used to get the flow patterns on suction and pressure sides of the plate for subcritical and supercritical regimes and to find the changes on these patterns when the Reynolds number is varied and the flow behaviour is changed from one regime to another. The pressure measurements were used to evaluate the average normal force acting on the plate at different Reynolds numbers and different angles of attack. The hot-

wire measurements were used to determine the mean central wake boundaries at two different Reynolds numbers for subcritical and supercritical regimes.

This investigation leads to the following results :

1)- For subcritical and supercritical regimes the mean pressure coefficients on the suction and pressure sides of the plate are not affected appreciably by the variation in Reynolds number for the same angle of attack. However, for the same Reynolds number, the influence of varying the angle of attack is quite significant for subcritical regime and reduced significantly for supercritical regime. This indicates that the normal force coefficient is hardly affected by the change in Reynolds number for the same angle of attack in both regimes. However, for a fixed Reynolds number , the influence of changing the angle of attack on the normal force seems to be more pronounced in the subcritical regime than it is in the supercritical regime.

2)- The influence of varying the Reynolds number on the percentage drop in the normal force is quite cosiderable as Reynolds number ranges between Re_c=o.5x 10^5 and 1.5x 10^5, however, in the range between Re_c=1.5x 10^5 and 3.7x 10^5 the

influence is reduced quite significantly.

3)- The change in Reynolds number does not have any significant influence on the shapes of the wake boundaries for the same angle of attack.

4)- The wake widens up when the angle of attack is changed from subcritical value to supercritical value for the same Reynolds number.

5)- For both subcritical and supercritical regimes the separation line between the two foci and observed on the suction side of the plate seems to move towards the leading edge as Reynolds number is increased for the same angle of attack.

6)- The flow pattern is changed between $\alpha=28^{o}$ and 32^{o} and the critical angle of attack was observed to be about $\alpha=30^{o}$, for all Reynolds numbers cosidered.

7)- The highly three-dimensional separation line observed on the suction side near the leading edge in subcritical regime seems to get closer to a two-dimensional separation line in the supercritical regime.

8)- The angle of attack seems to play a crucial role in the way the flow behaves over the plate.

List of References

(1). Ahlborn F.," Hydrodynamisch Experimentaluntersuchungen " Jb. Schiffbautechn. Ges.,Vol.5, 1904, PP. 417-447.

(2). Ahlborn F.," Die Wirbelbildung im Widerstandsmechanismus des Waseers ", Jb. Schiffbautechn. Ges., Vol.6, 1905, PP. 67-81.

(3). Ahlborn F. ," Die Widerstandsvorgang im Wasser anPlatten und Schiffskorpern " , Die Entstehung der Wellen , JB. Schiffbautechn Ges., Vol. 10, 1909, PP. 370-431.

(4). Budair M.U.,Mahmood M., and Abu-Saleh M.K., " Experiments on Flat Square Plate at High Angles of Attack",Mechanical Engineering Departement, U.P.M.,Seconed Saudi Engineering Conference, Vol.3 , PP.1493-1510, Dhahran, Saudi Arabia , 1985.

(5). Budair M.U.,Ayoub A.,and Karamcheti k. ," An Experimental Investigation of the Flow Past a Finite Circular Cylinder at a low Subcritical Reynolds Number",Stanford University, Departement of Aeronutics and Astronautics, June 1981 , NASA.

(6). Calvert, J.R. " Experiments on the Flow Past an Inclined Disc " Journal of Fluid Mech., Vol.29, 1967, PP. 691-703.

(7). Dines W.H. " On Wind Pressure upon an Inclined Surface ", Proc. Roy. Soc. London, Vol. 48, 1890 , PP. 235-257.

(8). Eden C.G., " Investigation by Visual Photographic Methods of the Flow Past Plates and Models ", A.C.A.,R.M.58,1912.

(9). Fage A. & Johansen,F.C. "On the Flow of Air Behined Flat Plate of Infinite Span ",ARC, R&M 1104,1927.

(10).Fail R., Lawford , J. A. , & Eyre, R. C. W., " Low-Speed Experiments on the Wake Characteristics of Flat Plate Normal to an Air Stream ", ARC,R&M. 3120-1959.

(11).Goldstein S.," Modern Developments in Fluid Dynamics " , Vol.II, Clarendon Press, Oxford ,1983 , and Dover publ. , New York, PP.3-16 , 1965.

(12).Hoerner S.F., " Drag of Various Types of Plats ",In Fluid Dynamic Drag, 2nd Ed. Publ. by Auther, New York,1965 ,PP. 3-16.

(13).Minor S.E.,Strikland J.H.,and Vann W.P.," Wind Effects on

Solar Tower Generators",Final Rept. on Task VII on D.O.E. Cotract EG-&&-01-3974 , Texas Tech. University, May 1979, PP.2 .

(14).Mahmood M.," Low-Speed Experiments on a Flat Square Plate at High Angles of Attack "MS Dissertation, UPM,Mechanical Engineering Department,Saudi Arabia 1984.

(15).Peckham D.H .," Low-Speed Wind-Tunnel Tests on a Series of Uncambered Slender Pointed Wings with Sharp edges " , Ministry of Aviation,Aeronautical Research Council Repor. and Memo.,R. M.No.3186, 1958 .

(16).Prandtl L., " Einige Fur Die Flugtechnik Wichtige Beziehungen aus der Mechanik " Etwas Uber den Luftwiderstand. Z.Flugtechnik Motorluftschiffahrt , Vol.1, 1910, PP.3-6 , 25-30 , 61-64 , 73-76 .

(17).Robert L., Stalling Jr. , " Reynolds Number Effects on Aerodynamic Chracteristics at Large Angle of Attack " NASA , Langley Research Center , Hampton , J.Spacecraft, Vol.17, No.2, March-April 1980 , Article No. 79-0301R , PP.129-133.

(18).Strickland J.H. , Matty R.R., and Barton G.H. , " Vortex

Shedding from Square Plates Perpendicular to a Ground Plane", AIAA Journal, Vol.18, 1980, PP. 715-716.

(19).Simmons L.F.G., Dewey N.S.," Wind Tunnel Experiments with Circular Discs ", ARC, R.M. 1334, 1931.

(20).Satya Pal. , " Free Stream Turbulence Effects on Wake Properties of Flate Plate at an Incidence " , Departement of Environmental Protection, New York, AIAA Journal, Vol. 23, No.12, PP.1868-1871,December 1985.

(21).Stanton T.E. and Marshaell D., "On the Eddy System in the Wake of Flat cicular Plates in Three Dimensional Flow " ARC,R.M.1358 , 1932 , also Pros. Soc.A. , Vol.130, 1931, PP. 295-301.

(22).Stahl W., and Mahmood M., " Some Aspects of the Flow Past a square Flat Plate at High Incidence " DFVLR, Aerodynamische Versuchsanstalt Gottingen, Institut fur Experimenetelle Stromungsmechanik, 1984.

(23).Van Westerhoven P., Wedemeger E., and Wendt J.F. , " Low Aspect ratio Rectangular Wings at High Incidence " in " Missile Aerodynamics ", AGARDCPP _ 336, 1982 , PP. 15-1 to 15-14.

(24).Winter H." Flow Phenomena on Plates and Airfoils of Short Span " NASA,TM 798, 1937.

(25).Winkelman A.E. and Balow J.B. , " Flow Field Model for a Rectangular Plan Form Wing Beyond Stall " AIAA Journal , Vol.18, 1980, PP. 1006-1008.

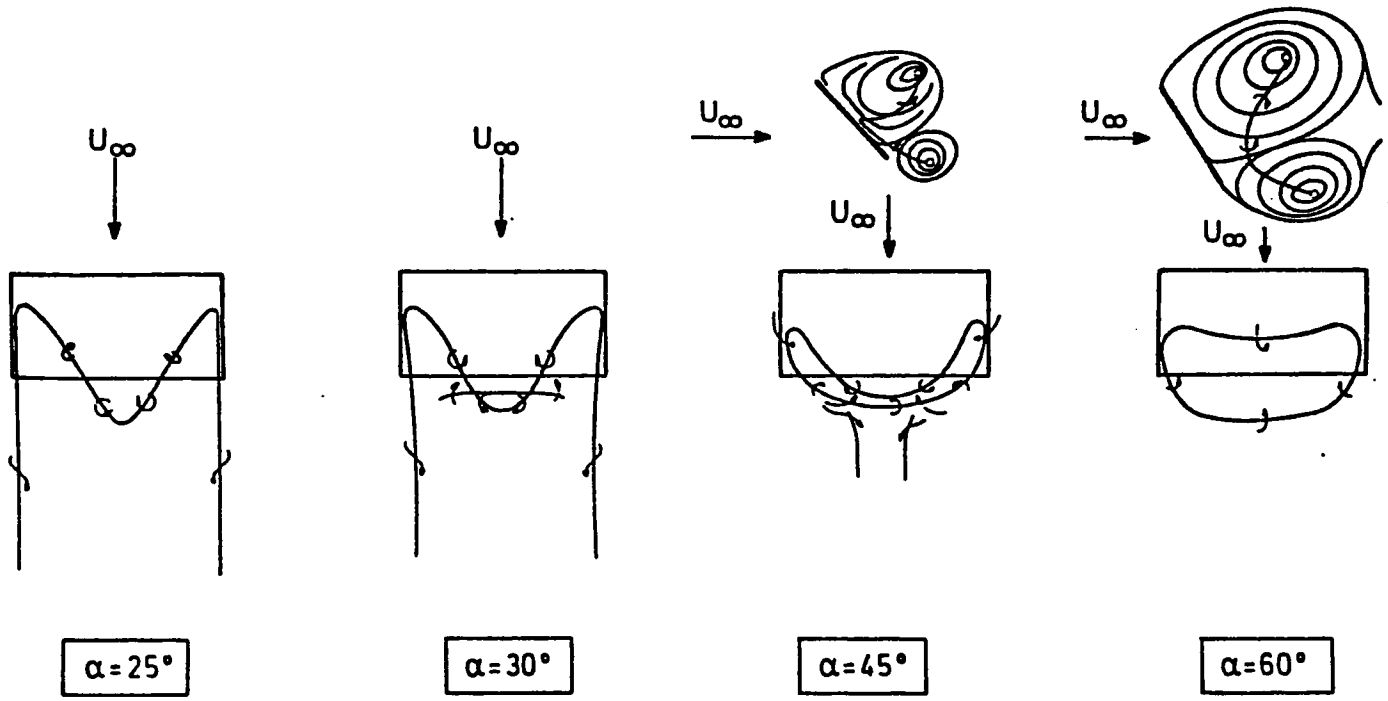

Fig. 1.1. Vortex pattern of rectangular plate, A = 2, at various incidences, acc. toF.Ahlborn [3].

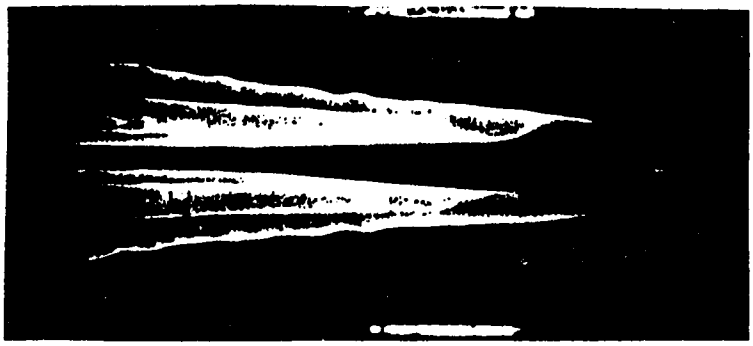

Fig.(1.2). Low velocity type of flow. Water

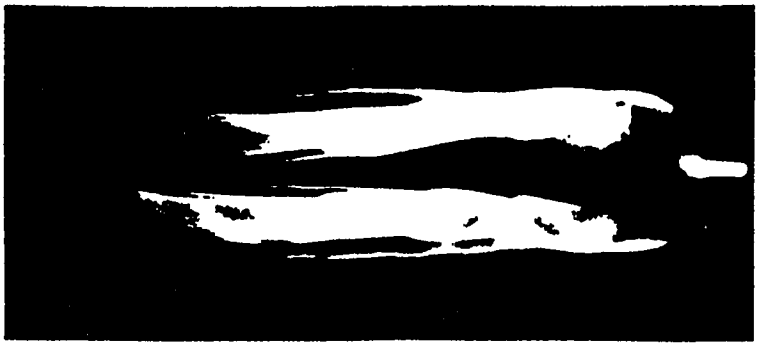

Fig.(1.3). Low velocity type of flow. Air.

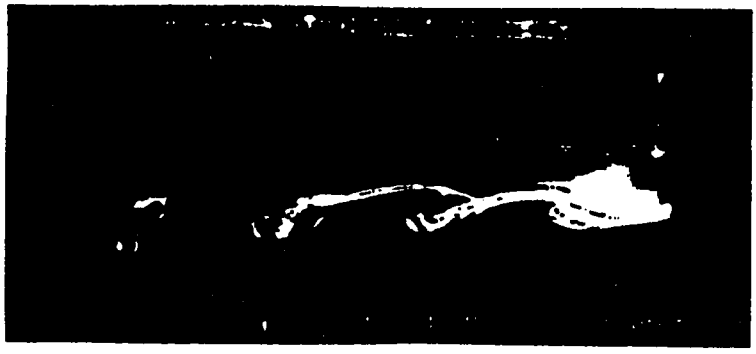

Fig.(1.4). High velocity type of flow. Water.

Fig.(1.5). High velocity type of flow. Water.

Fig.(1.6). High velocity type of flow. Air.

Fig.(1.7). High velocity type of flow. Air.

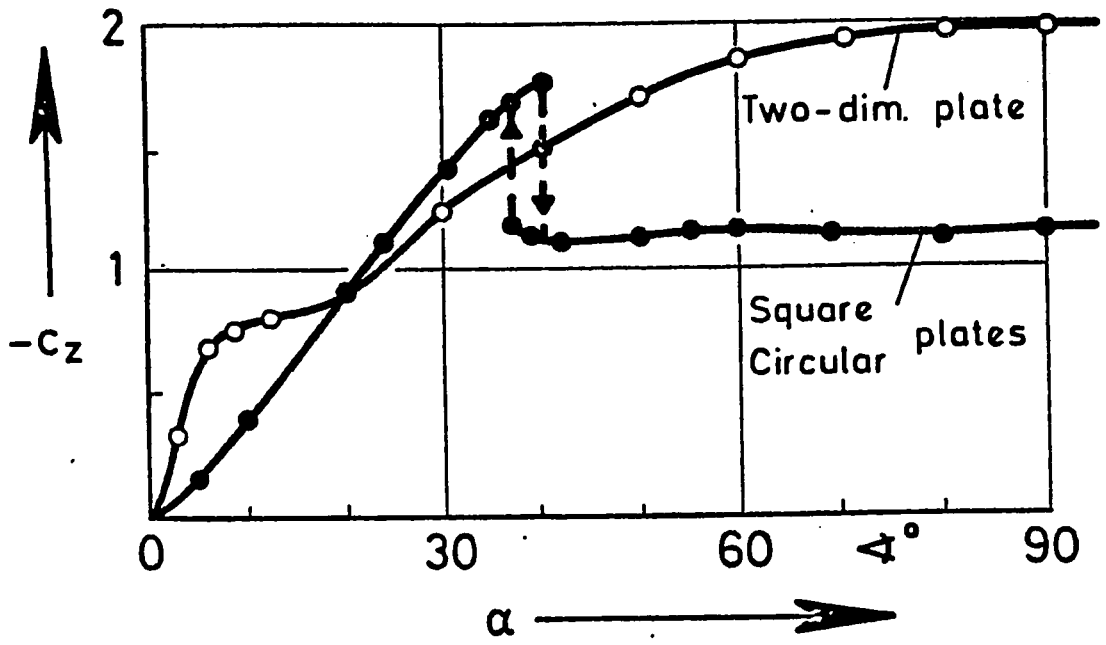

Fig.(1.8) Normal-force coefficients vs. incidence for two-dimensional, circular, and square plates, from S.F. Hoerner (12)

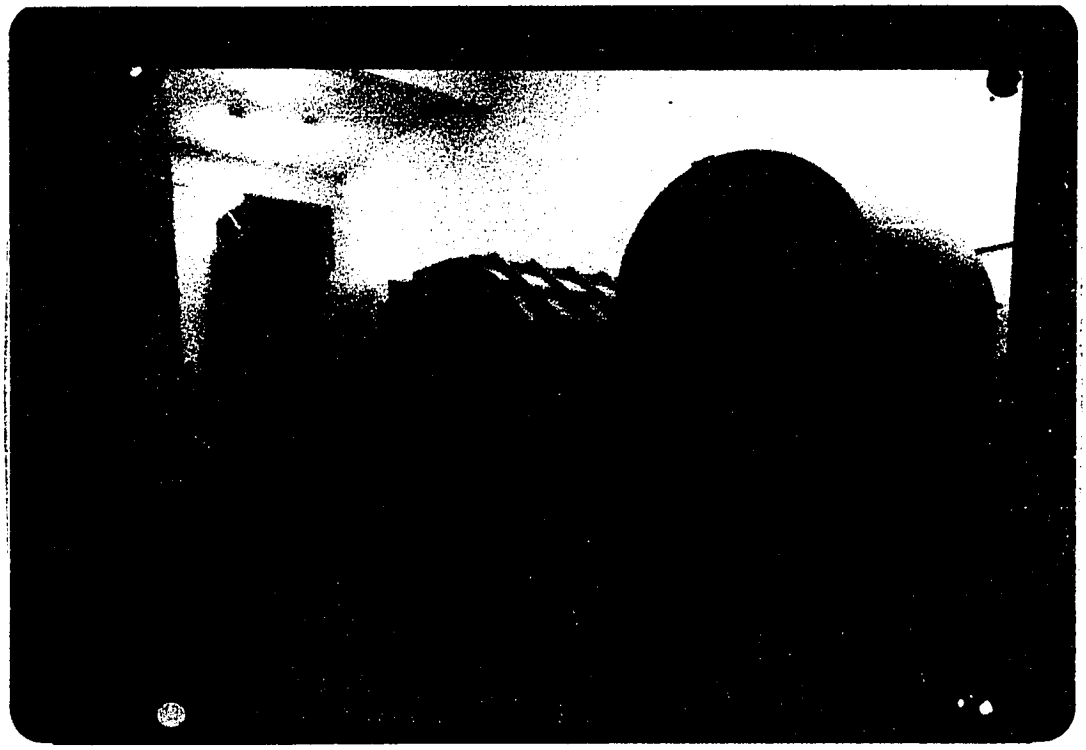

Fig.2.1. Wind tunnel.

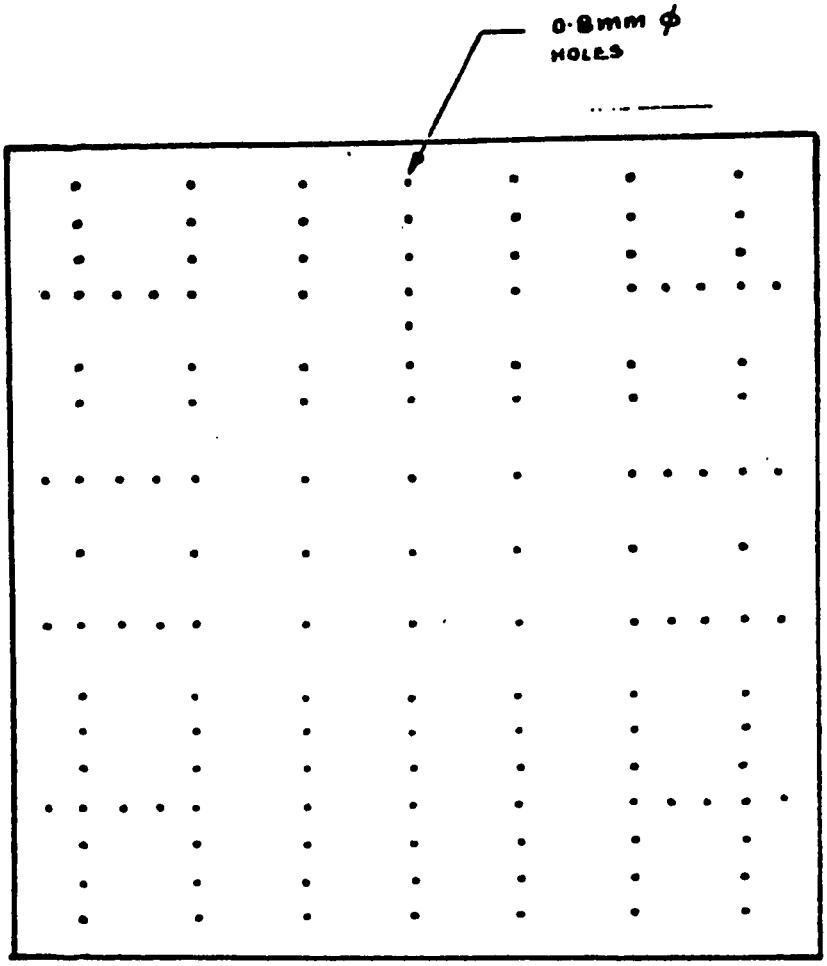

Fig. 2.2. Pressure holes on the plate.

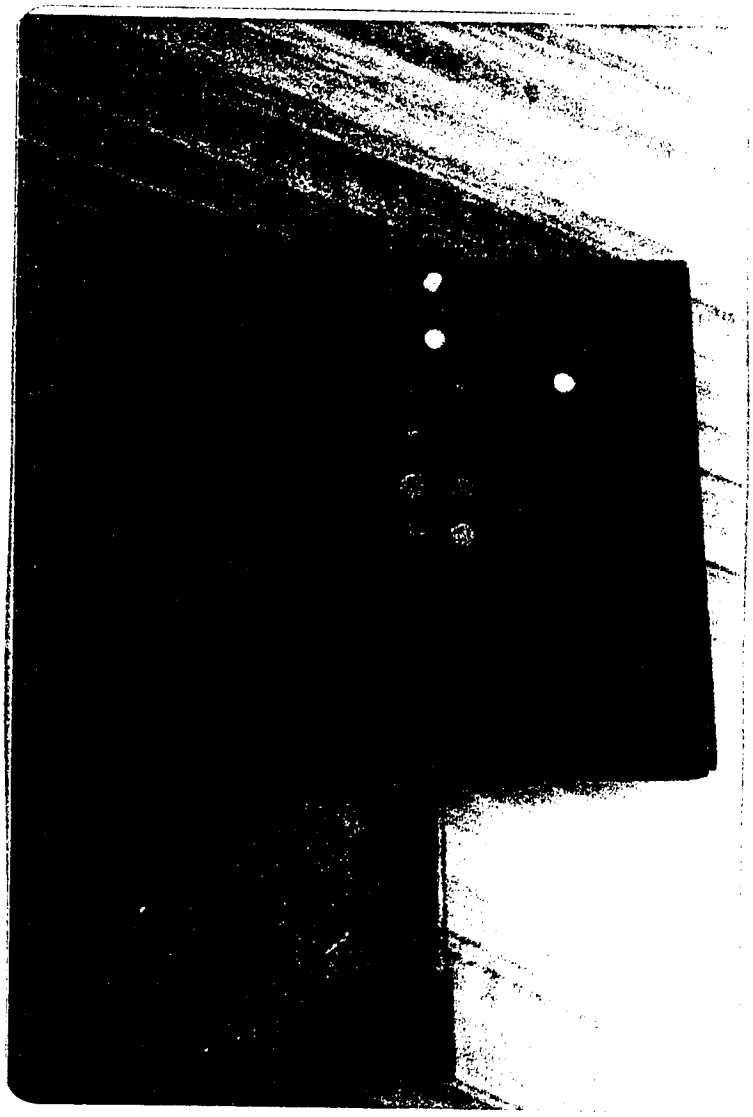

Fig. 2.3. Surface flow visualization model.

Fig. 2.4. Square plate pressure model.

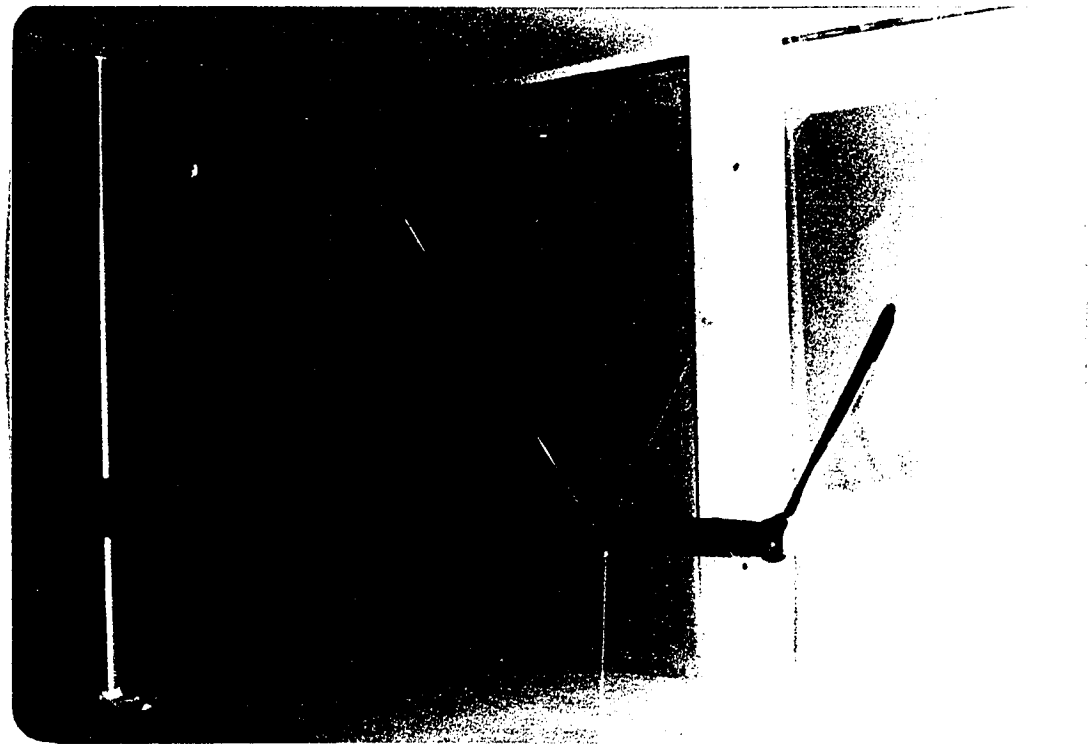

Fig.2.5. Surface flow visualization Set-up.

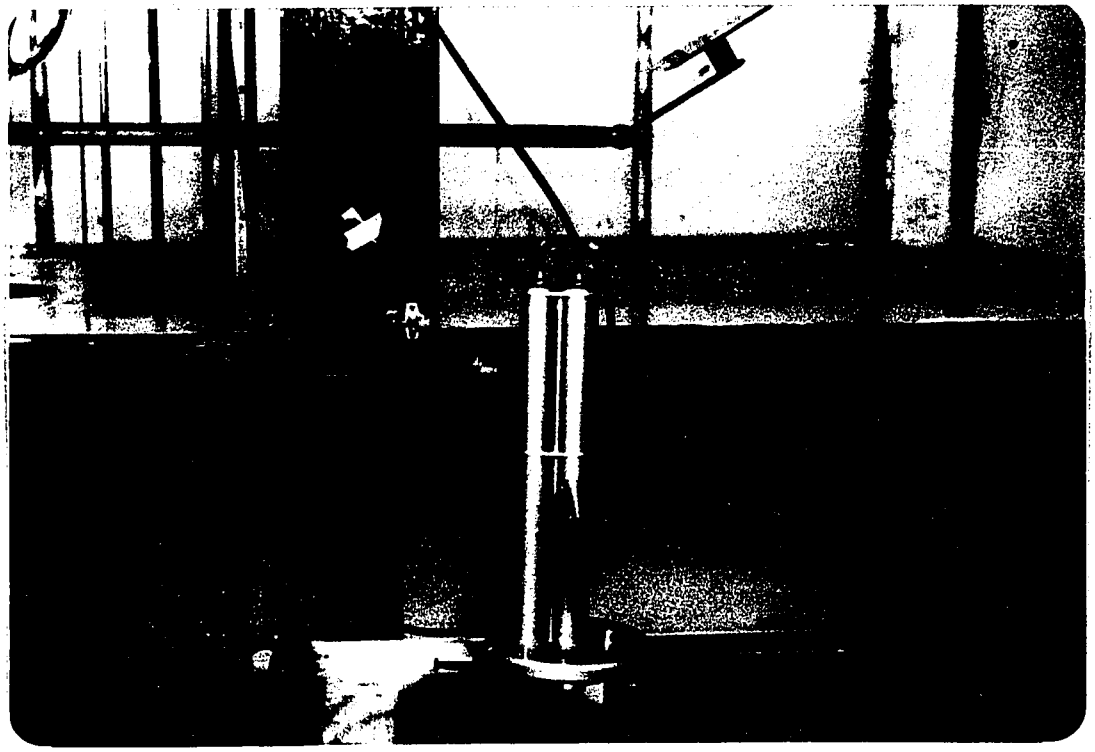

Fig.2.6. Manometer in operation

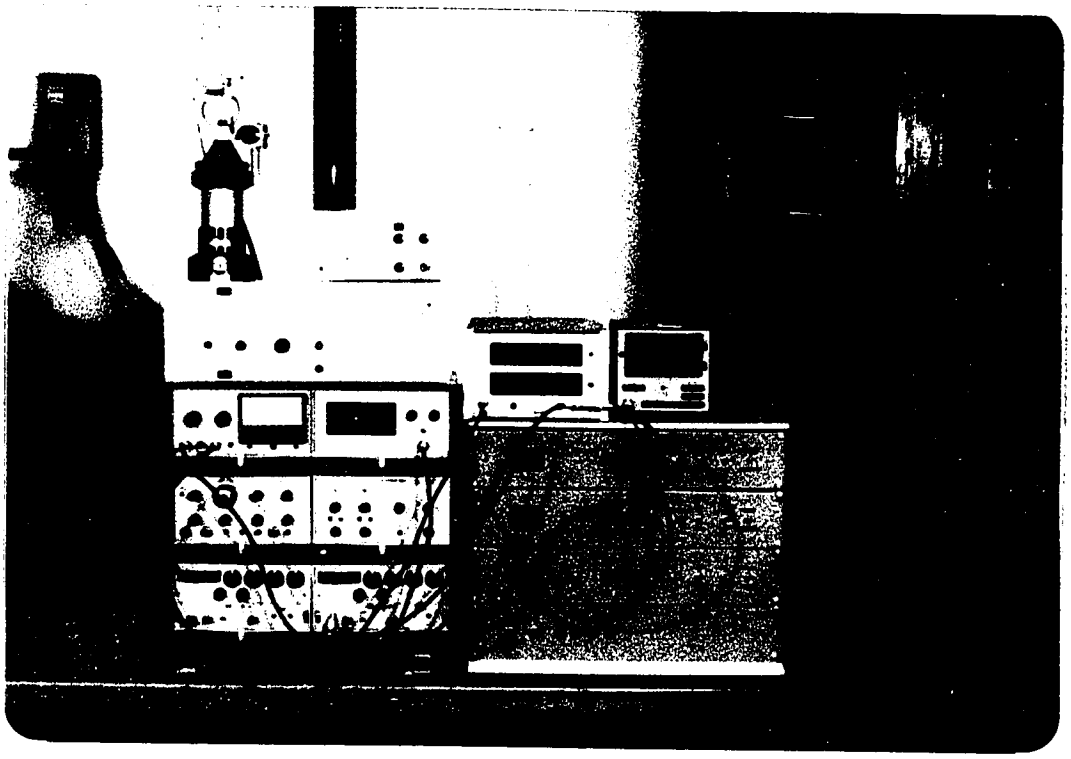

Fig.2.7. Hot-wire instrumentation.

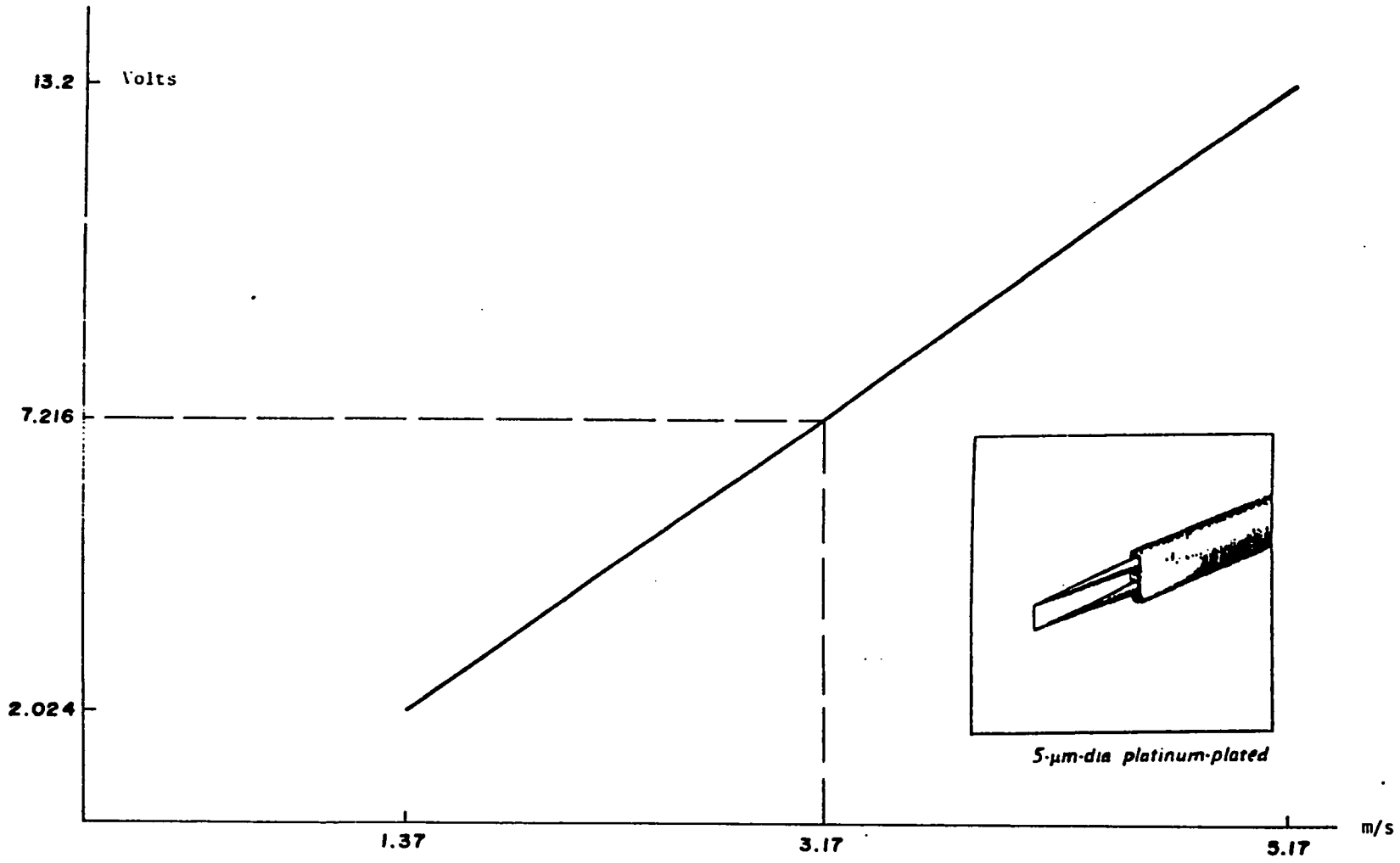

Fig. 2.8. Hot-wire calibration curve.

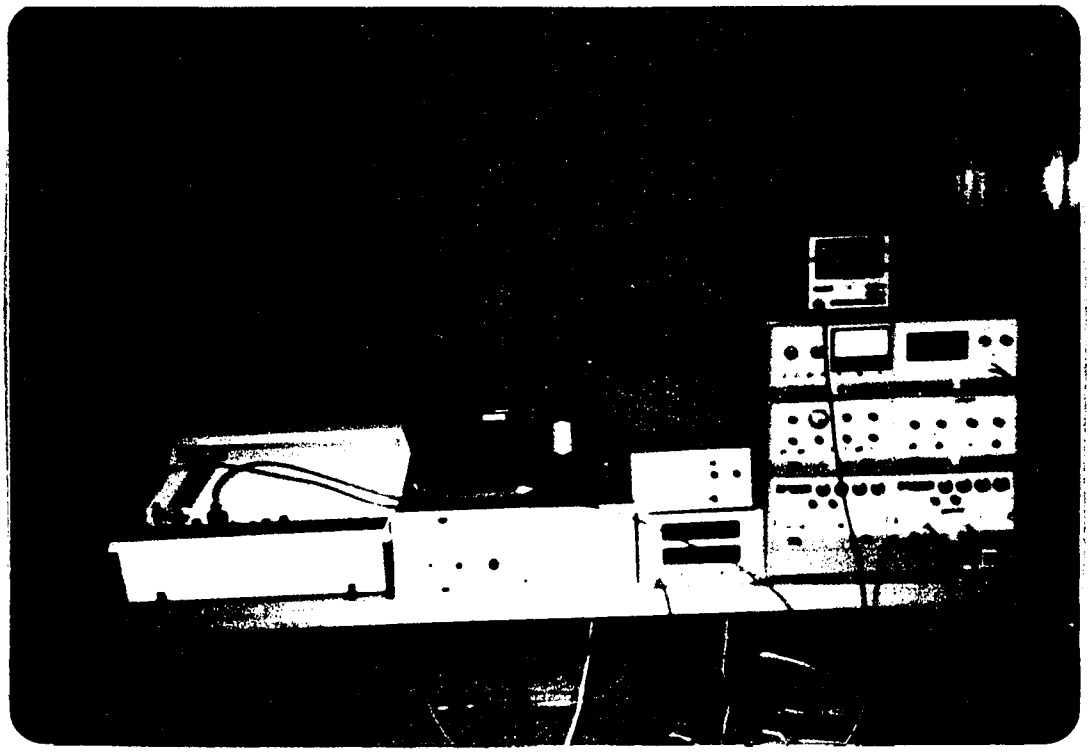

Fig.2.9. Hot-wire calibration equipment.

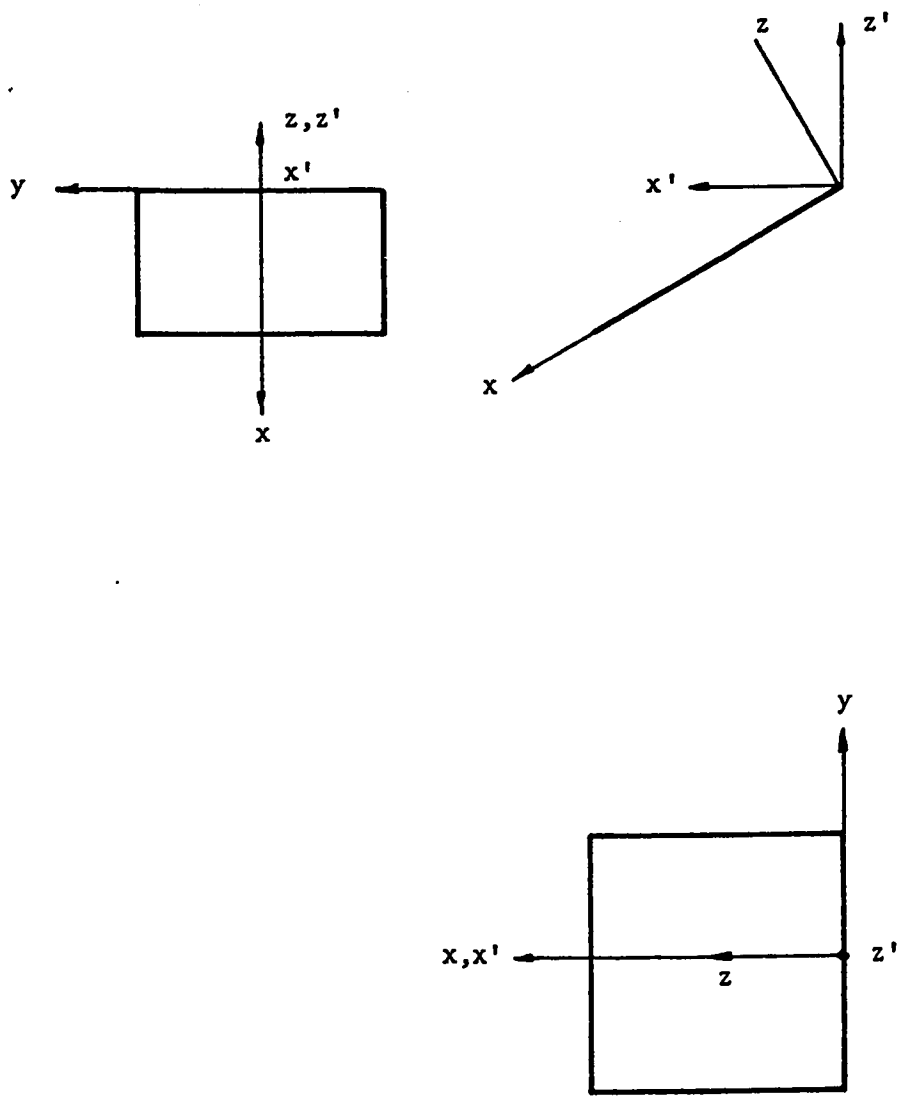

Fig. 2.10. The coordinate system.

Fig.2.11. Hot-wire measurements set-up.

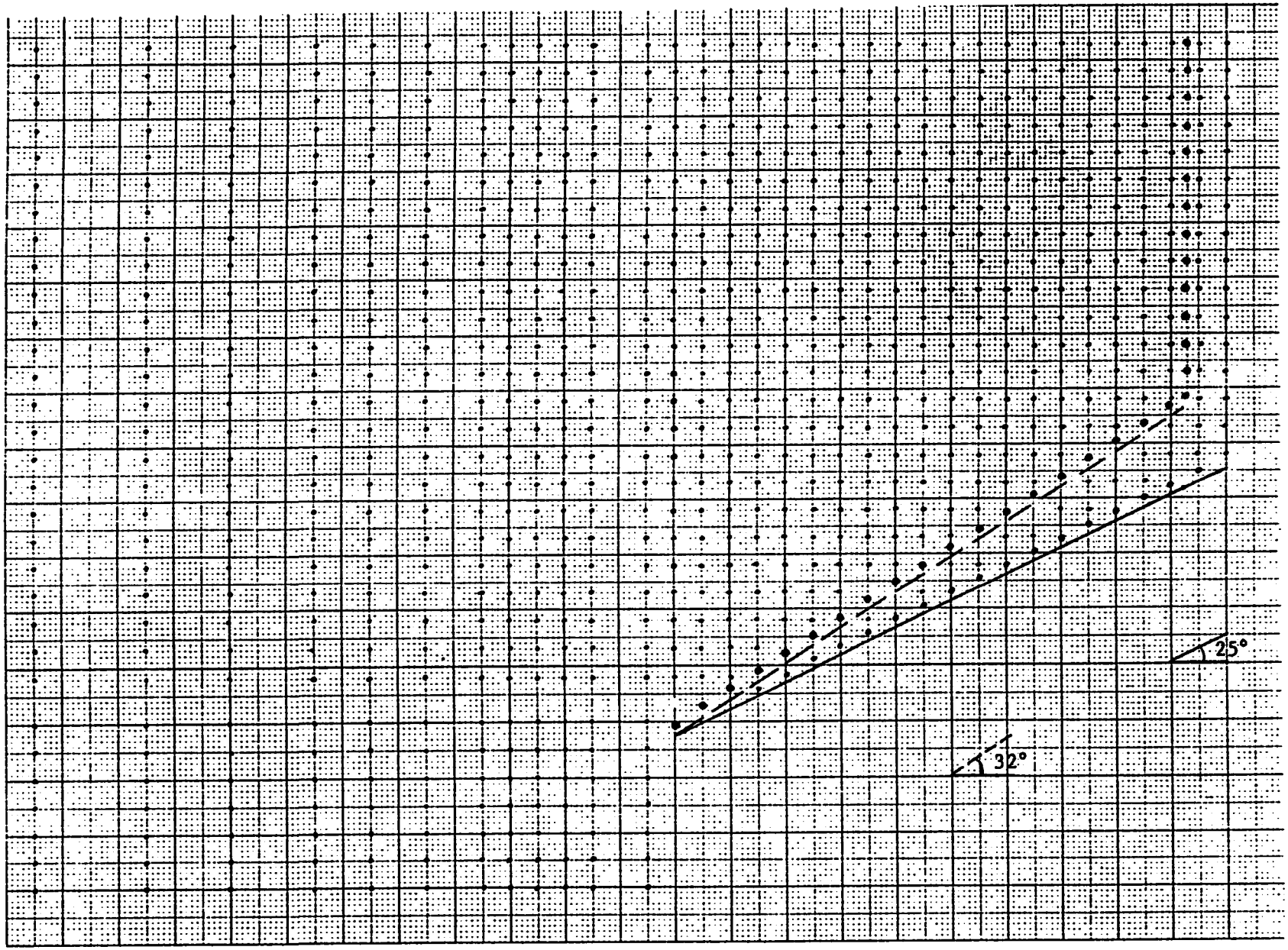

Fig. 2.12. Hot-wire measurements stations.

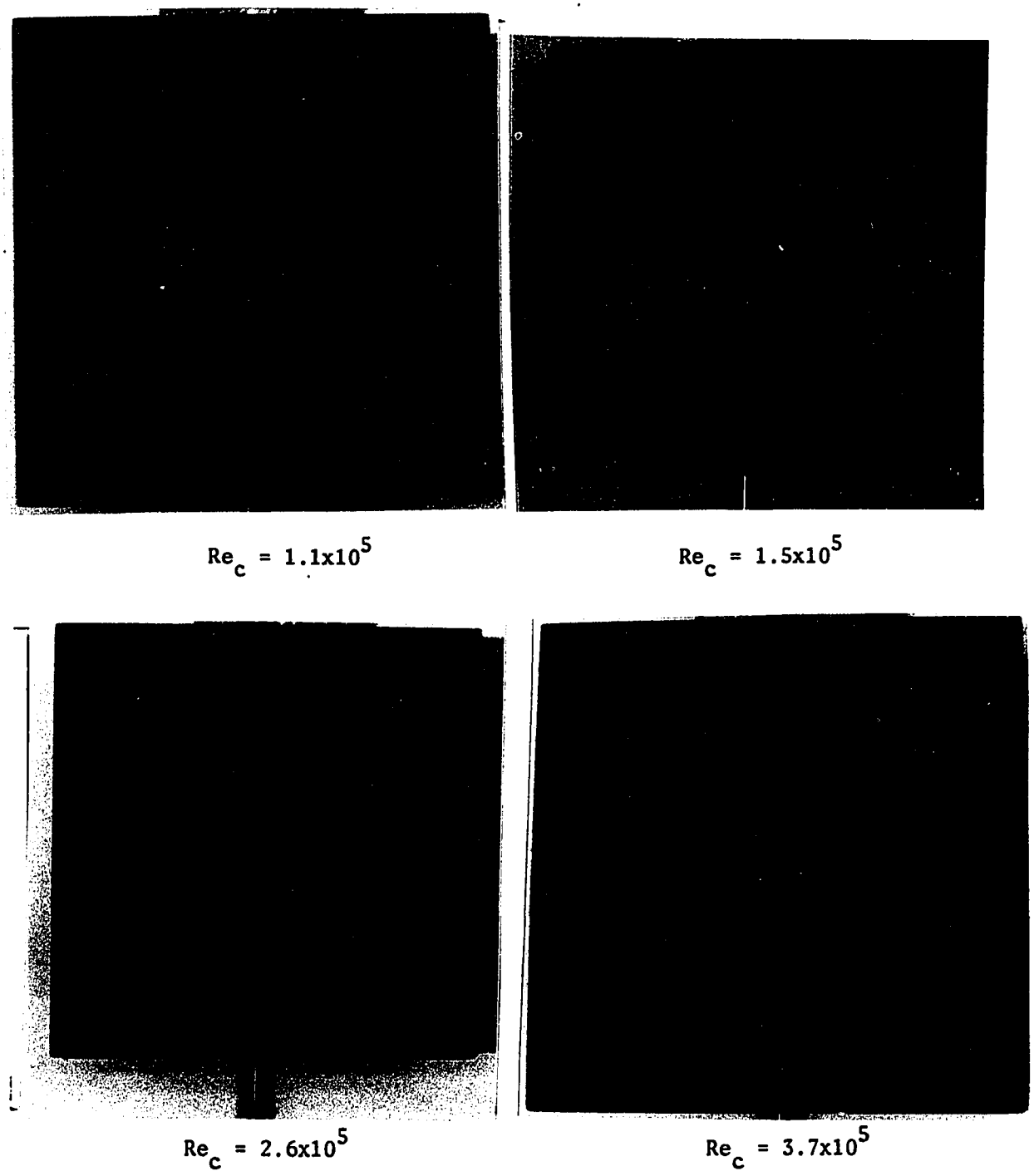

Fig. 3.1. Surface flow visualization on suction side for $\alpha = 25^o$.

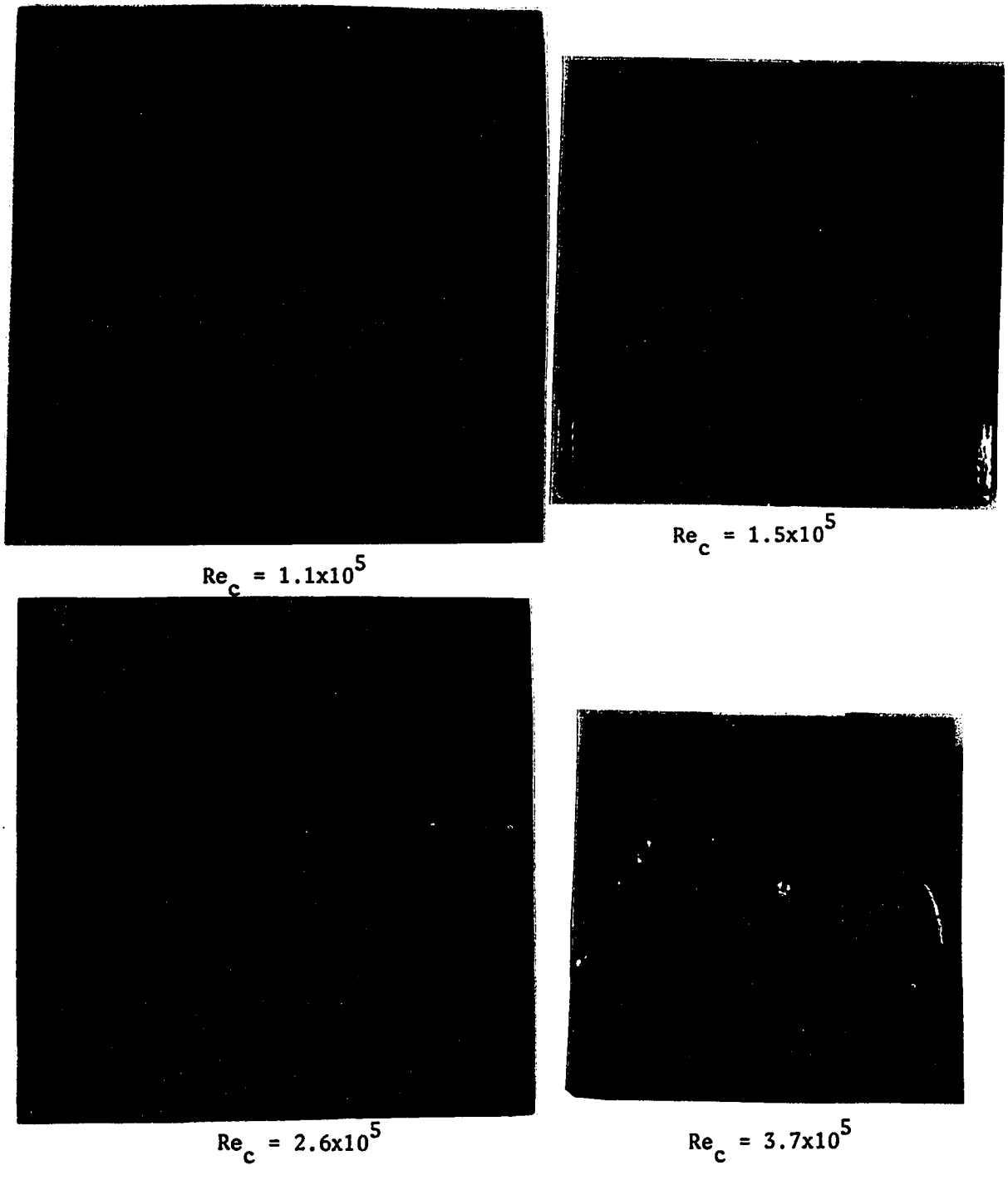

Fig. 3.2. Surface flow visualization on suction side for $\alpha = 28^o$.

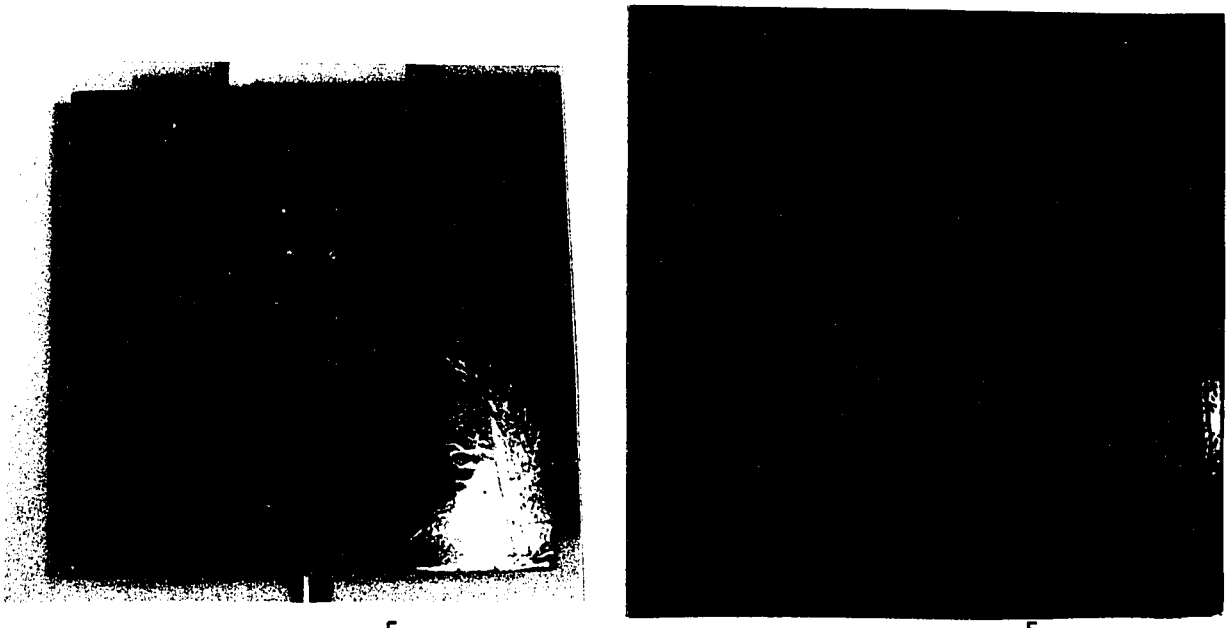

$Re_c = 1.5 \times 10^5$

$Re_c = 2.6 \times 10^5$

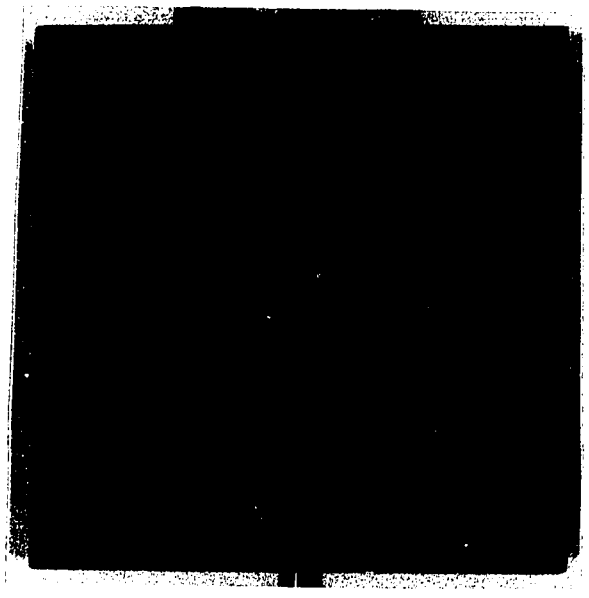

$Re_c = 3.7 \times 10^5$

Fig. 3.3. Surface flow visualization on suction side for $\alpha = 32^o$.

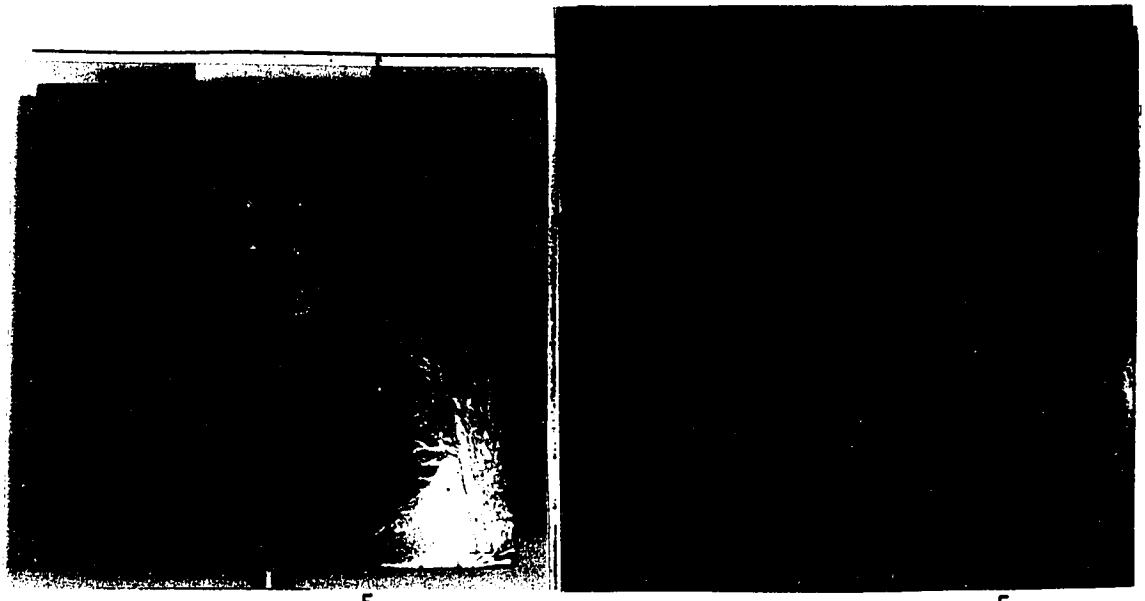

$Re_c = 1.5 \times 10^5$ $Re_c = 2.6 \times 10^5$

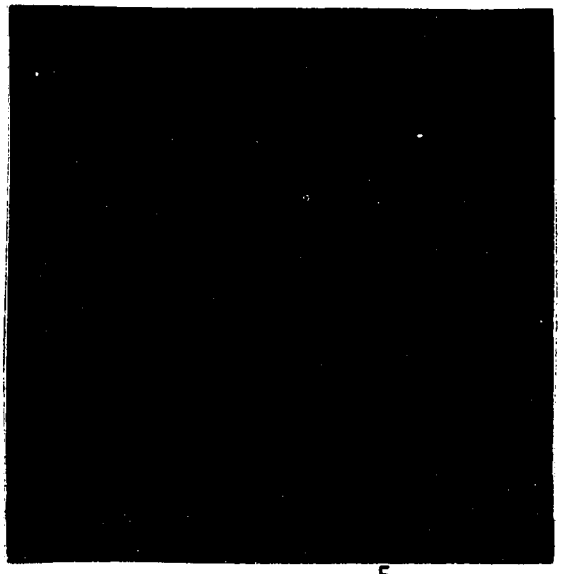

$Re_c = 3.7 \times 10^5$

Fig. 3.4. Surface flow visualization on suction side for $\alpha = 35^o$.

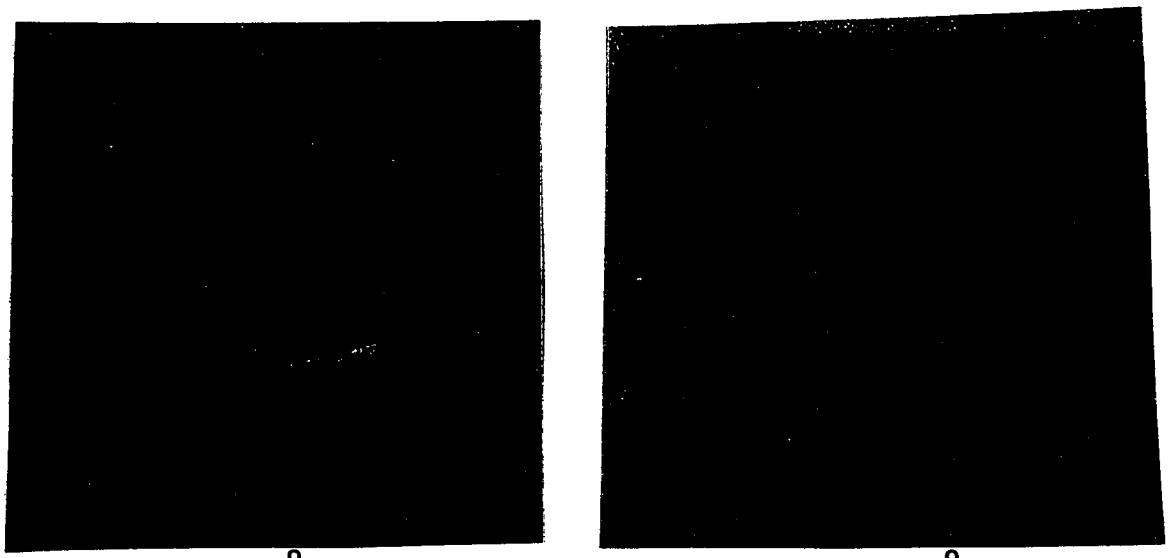

$\alpha = 28^{o}$ $\alpha = 32^{o}$

$Re_c = 2.6 \times 10^5$

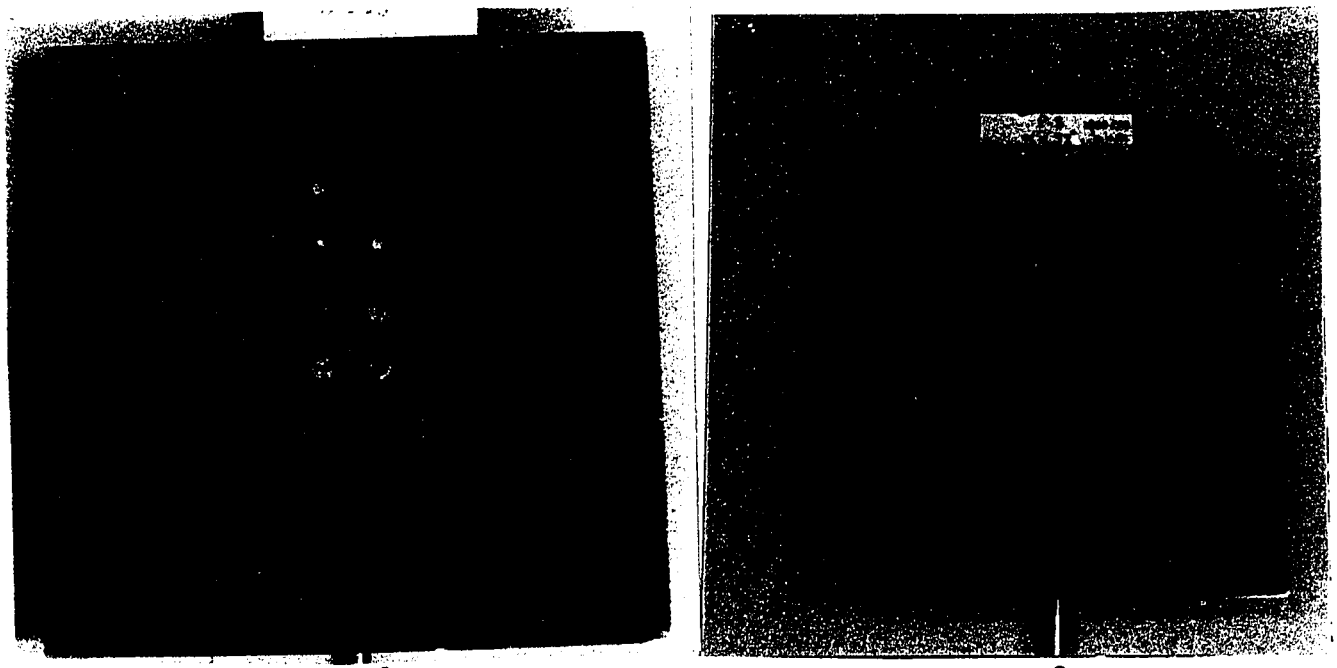

$\alpha = 28^{o}$ $\alpha = 32^{o}$

$Re_c = 3.7 \times 10^5$

Fig. 3.5. Surface flow visualization on pressure side.

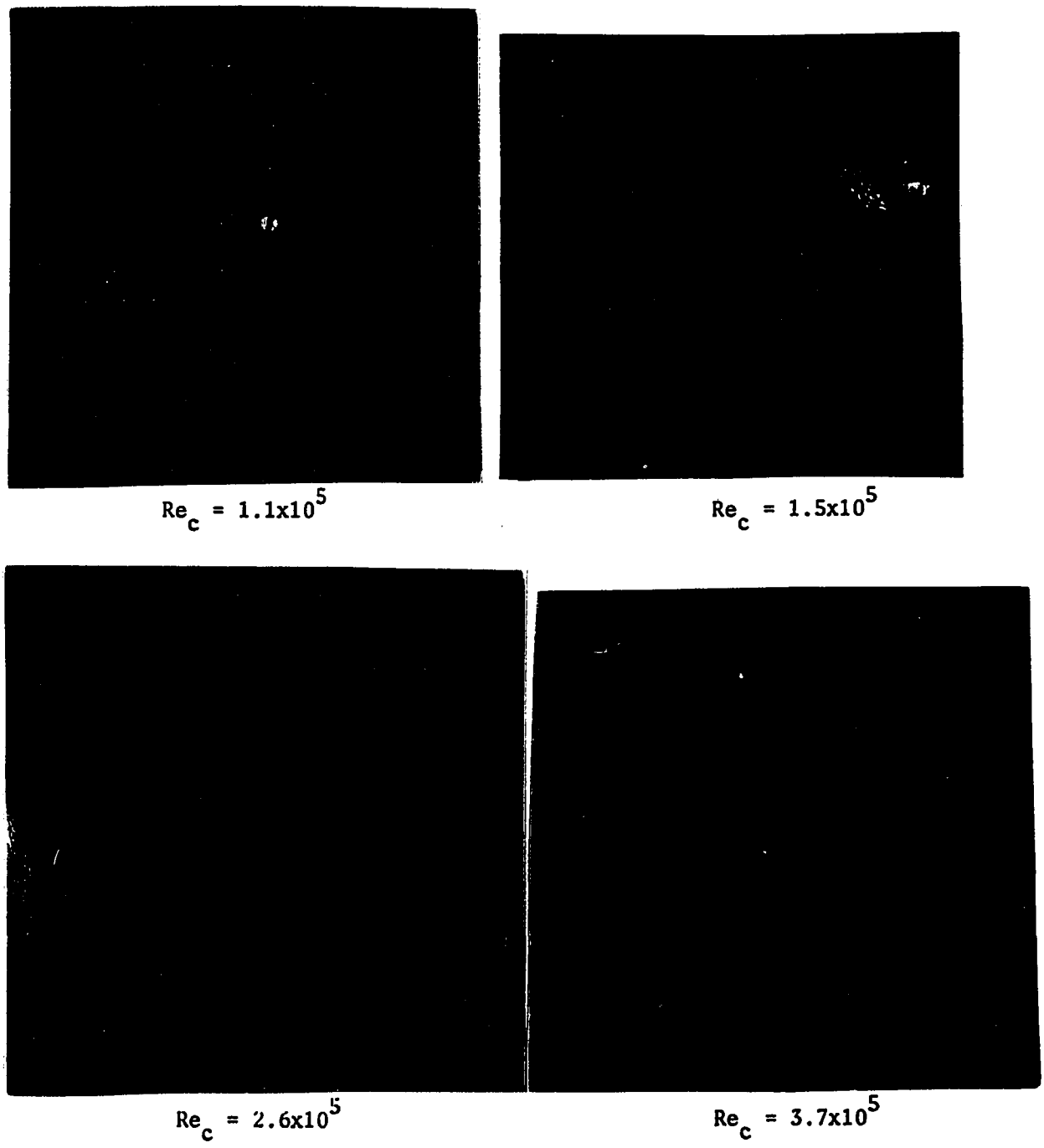

Fig. 3.6. Surface flow visualization on suction side for $\alpha = 30^o$.

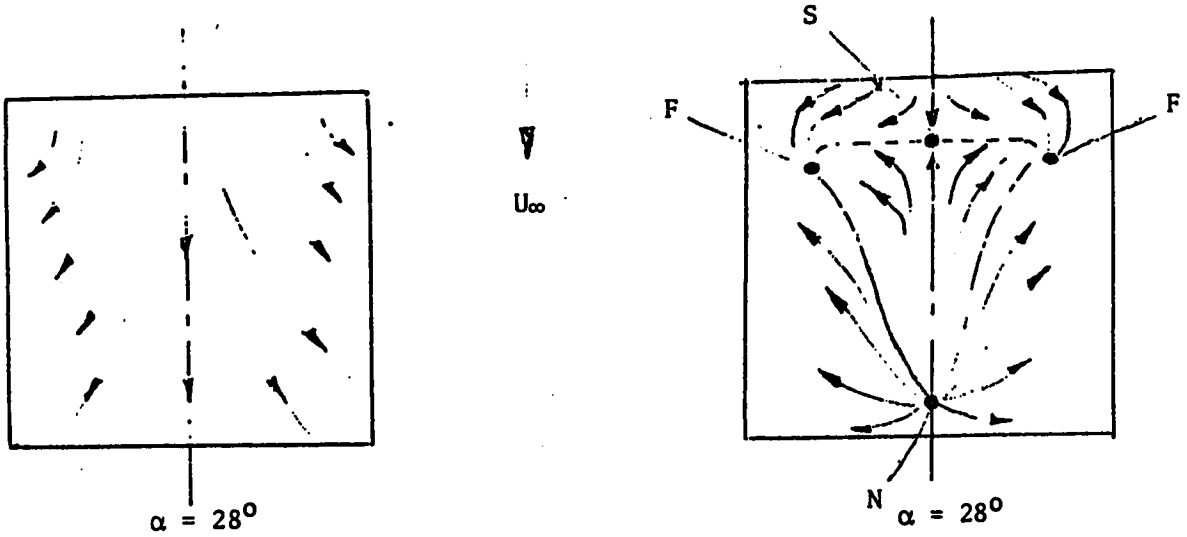

PRESSURE SIDE

SUCTION SIDE

F = FOCUS

N = NODE

S = SADDLE

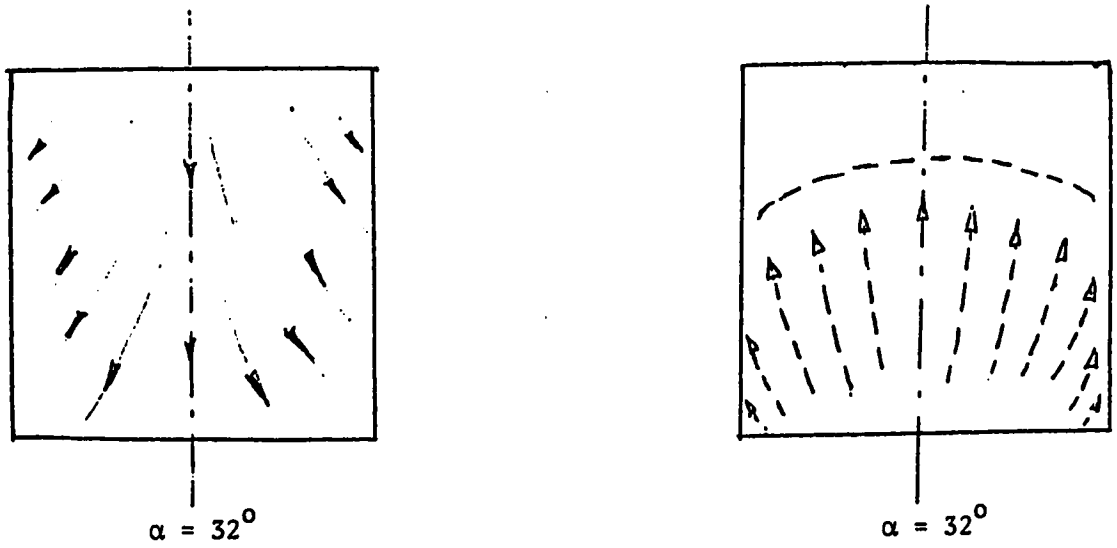

PRESSURE SIDE

SUCTION SIDE

Fig.3.7 Surface flow visualization for sub and supercritical incidence.

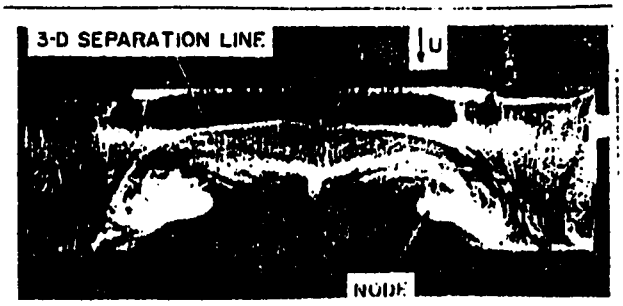

Fig.3.8. Oil flow patterns developed on a law aspect ratio wing (14% Clark Y airfoil) at α=22.8 deg. Re_c=245,000. A=3.5.

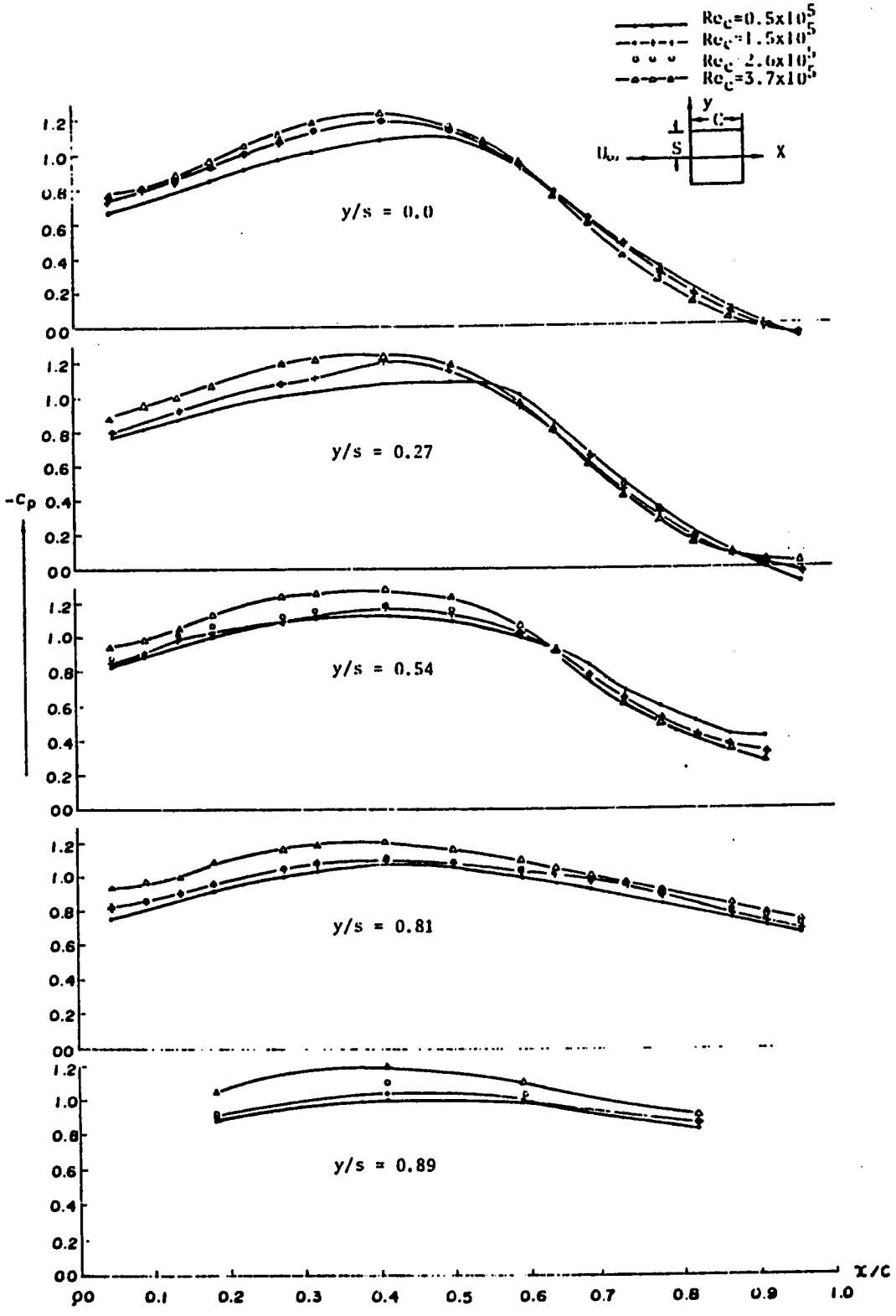

Fig. 3.9. Chordwise pressure distribution, $\alpha = 25°$. Suction side.

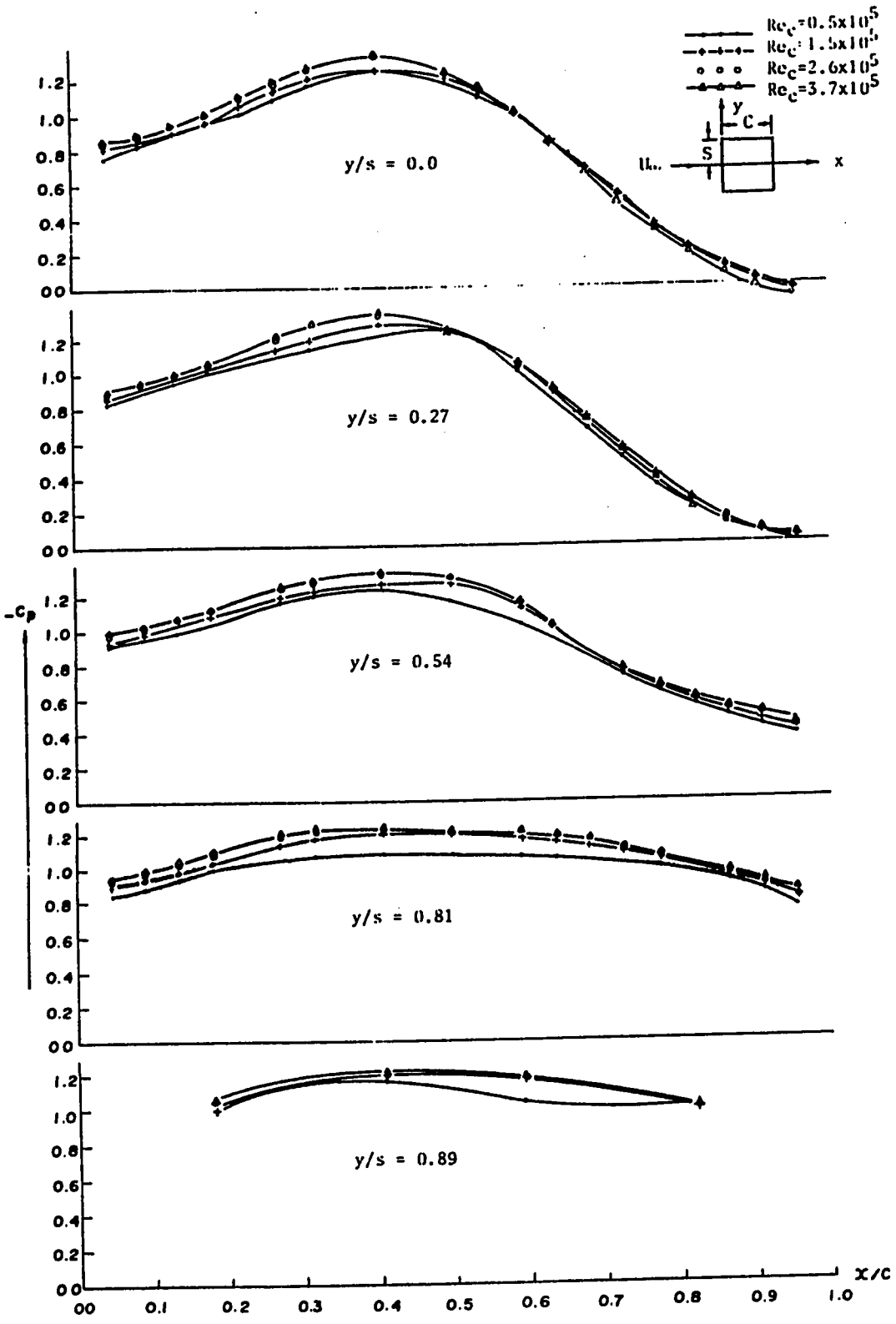

Fig. 3.10. Chordwise pressure distribution, $\alpha = 28°$. Suction side.

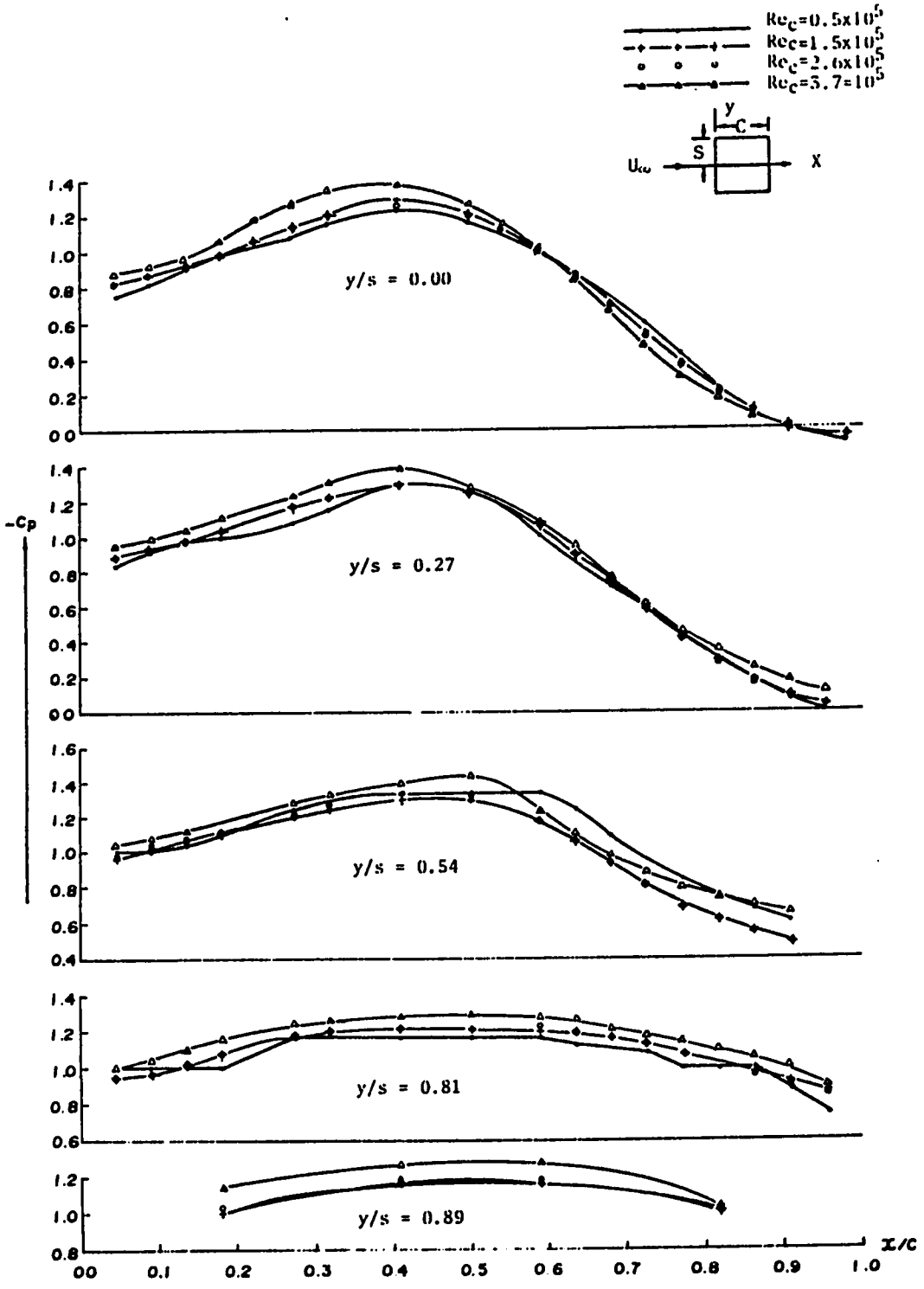

Fig. 3.11. Chordwise pressure distribution, $\alpha = 29°$. Suction side.

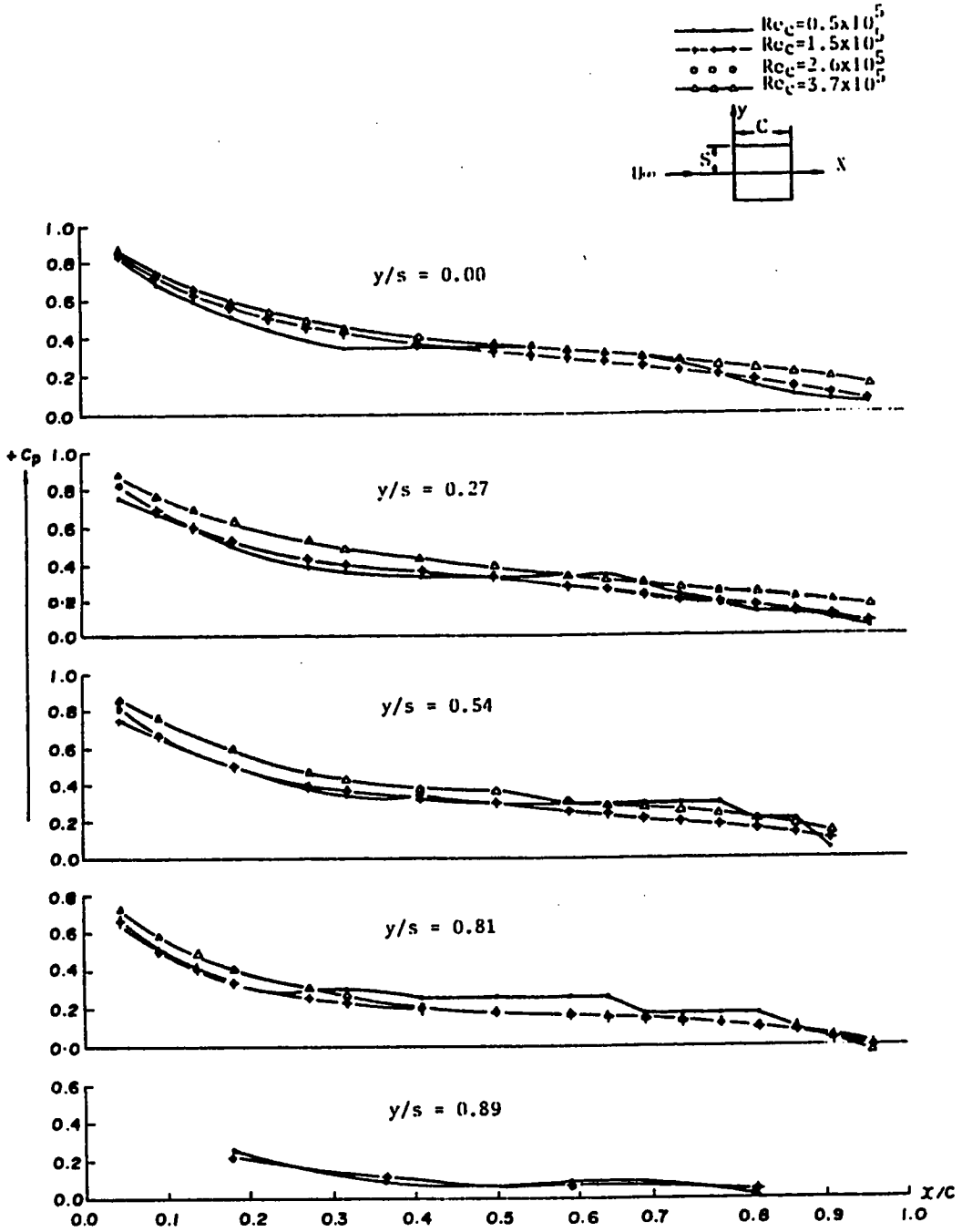

Fig. 3.12. Chordwise pressure distribution, $\alpha = 25°$. Pressure side.

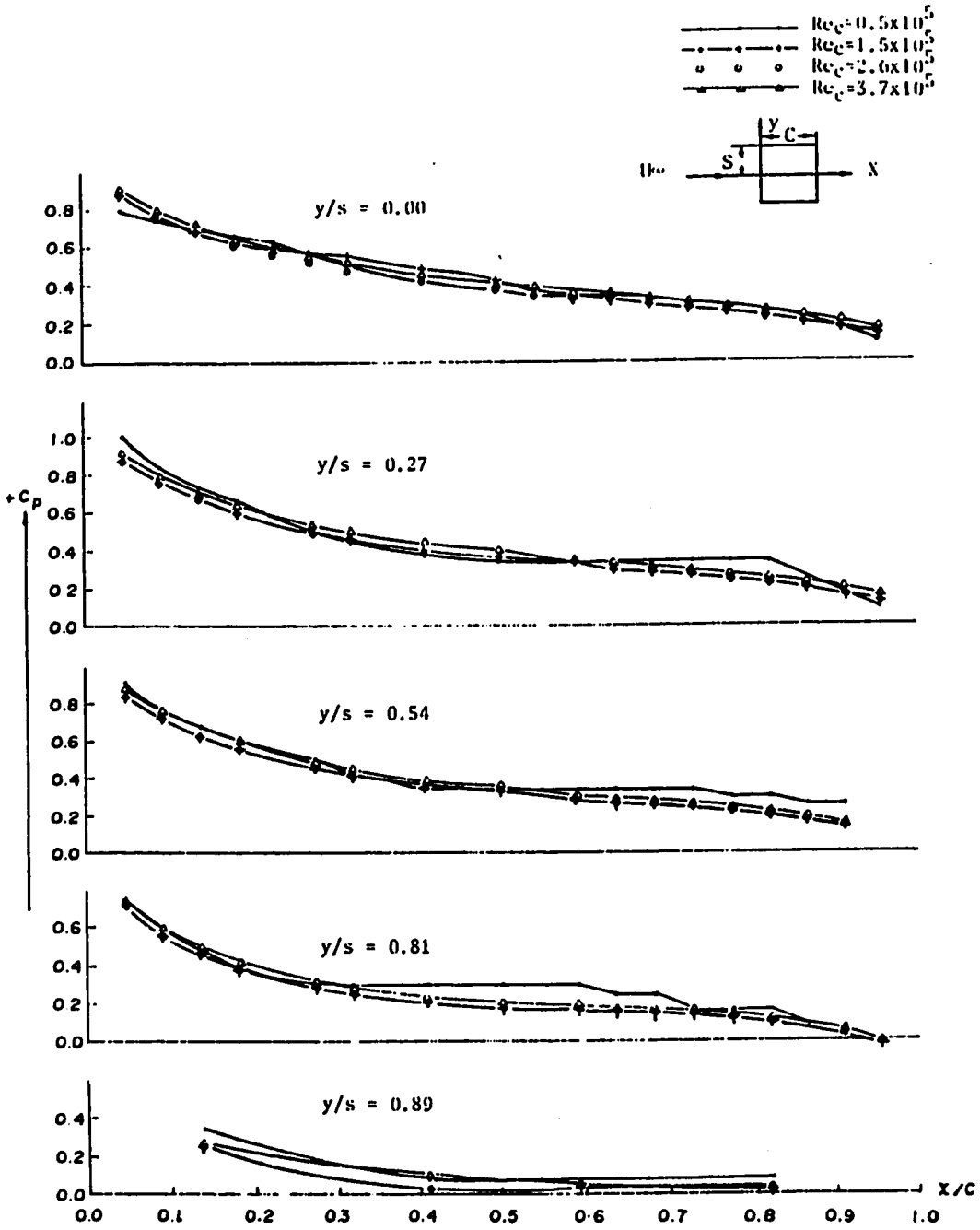

Fig. 3.13. Chordwise pressure distribution, $\alpha = 28°$. Pressure side.

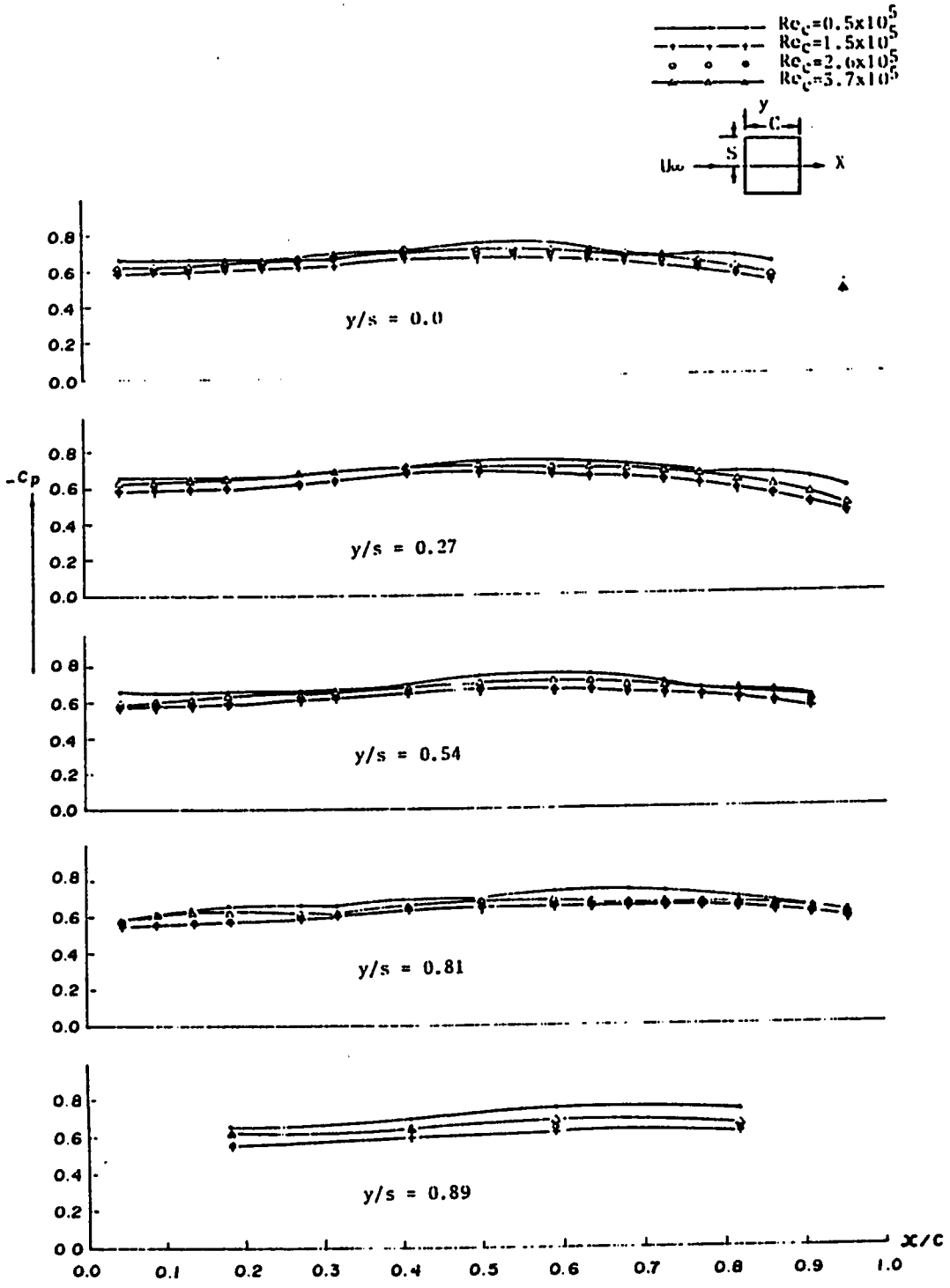

Fig. 3.14. Chordwise pressure distribution, α = 32°. Suction side.

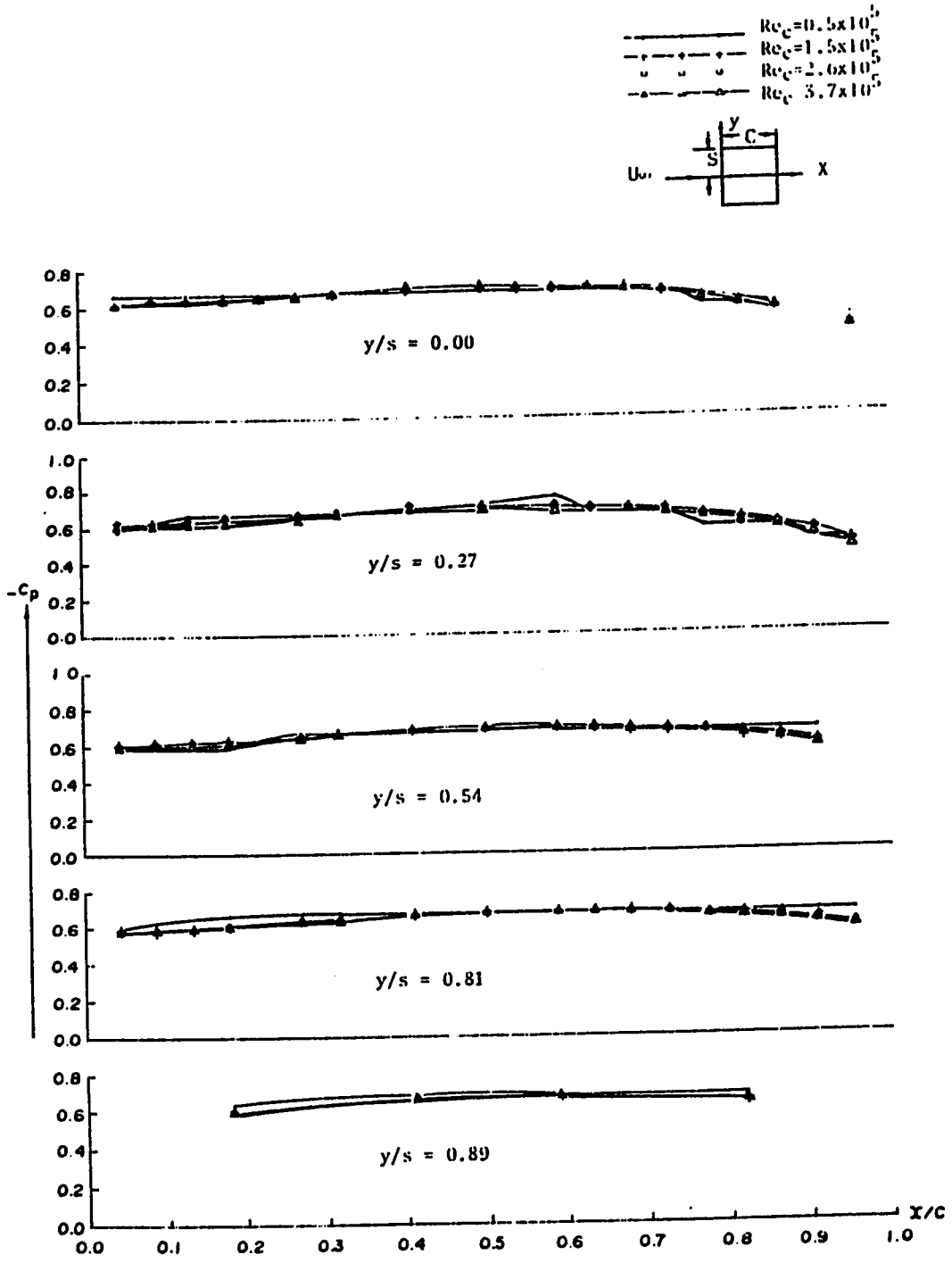

Fig. 3.15. Chordwise pressure distribution, $\alpha = 35°$. Suction side.

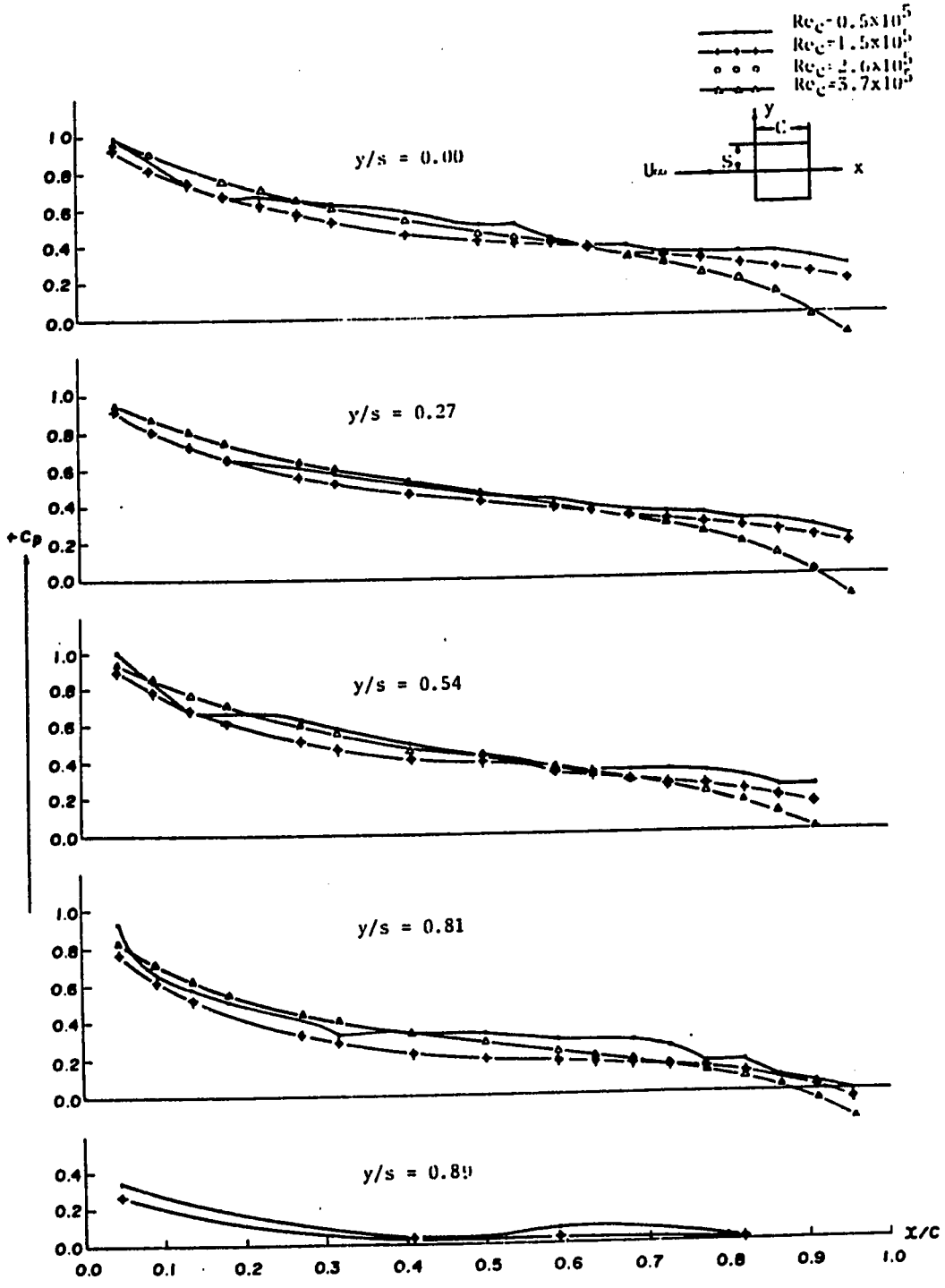

Fig. 3.16. Chordwise pressure distribution, $\alpha = 32°$. Pressure side.

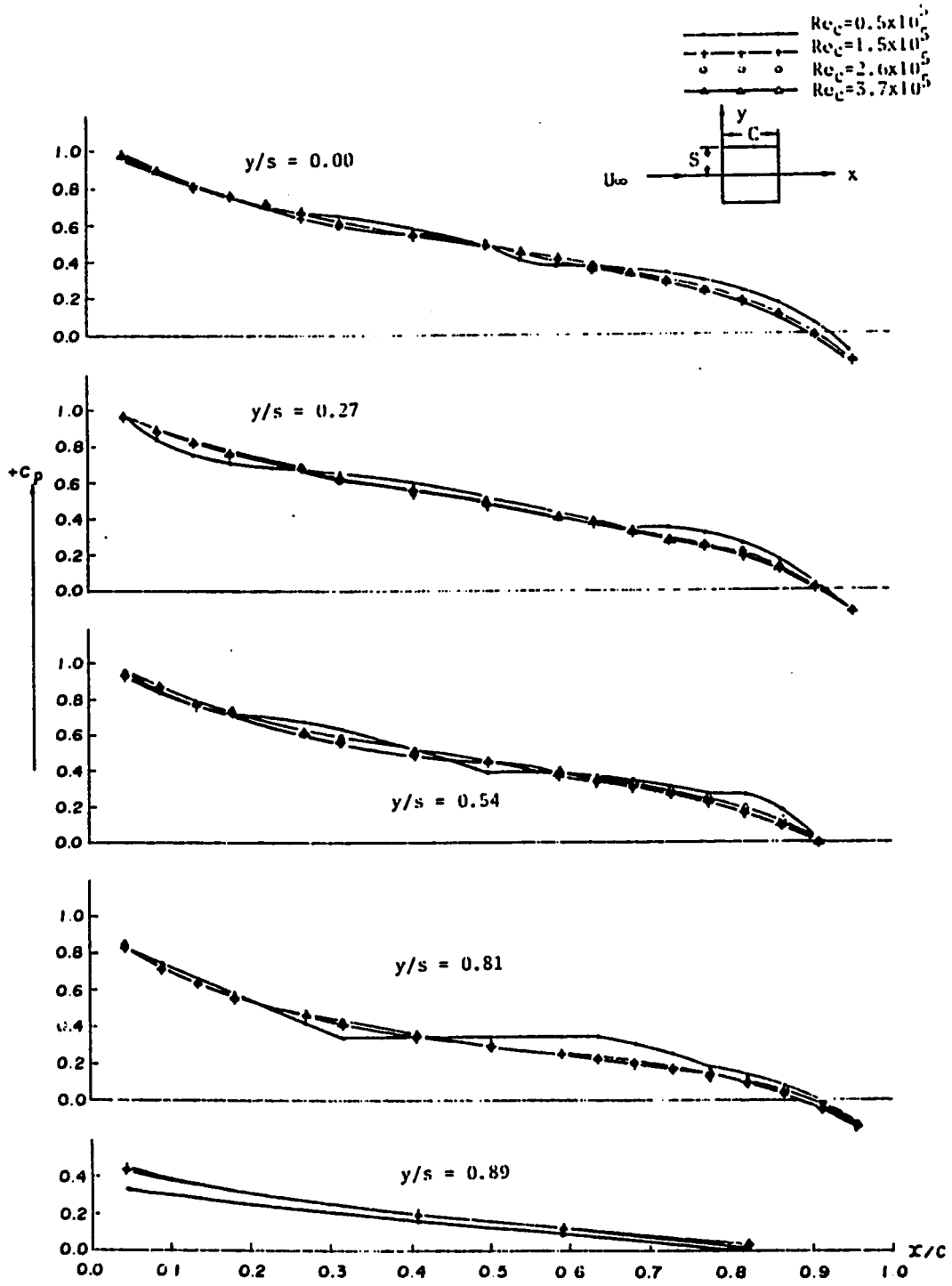

Fig. 3.17. Chordwise pressure distribution, $\alpha = 40°$. Pressure side.

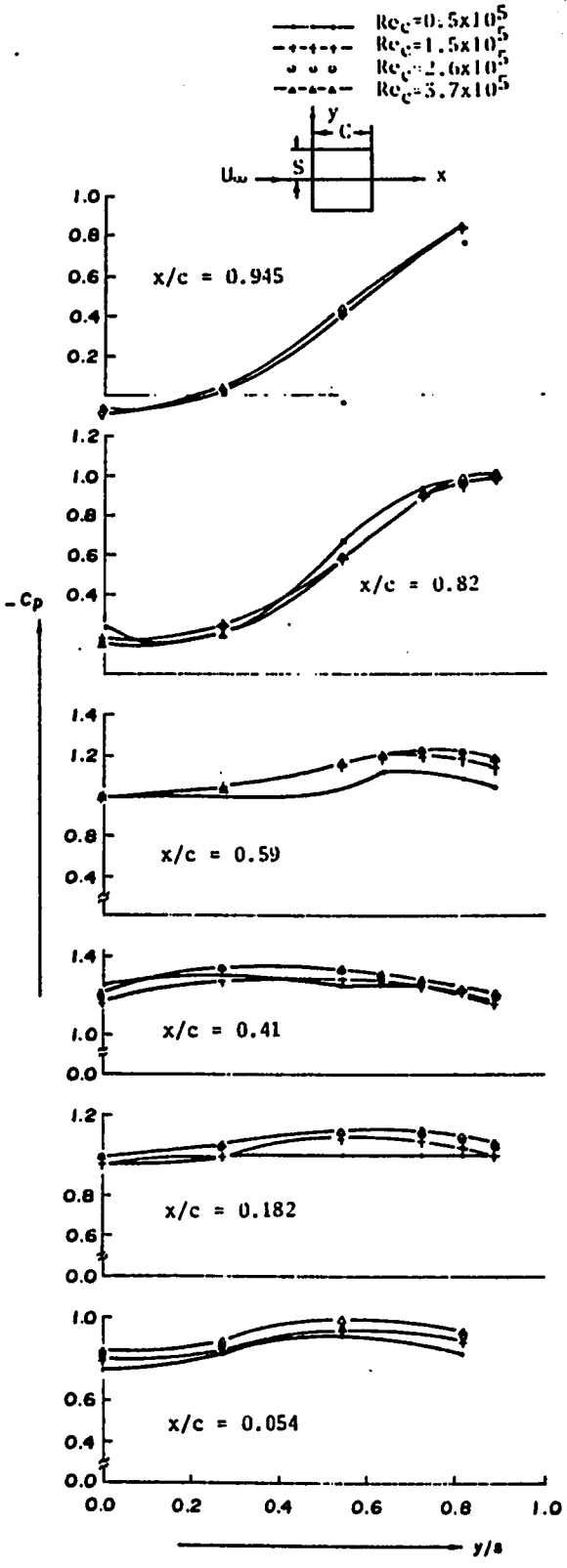

Fig. 3.18. Spanwise pressure distribution, $\alpha = 28°$. Suction side.

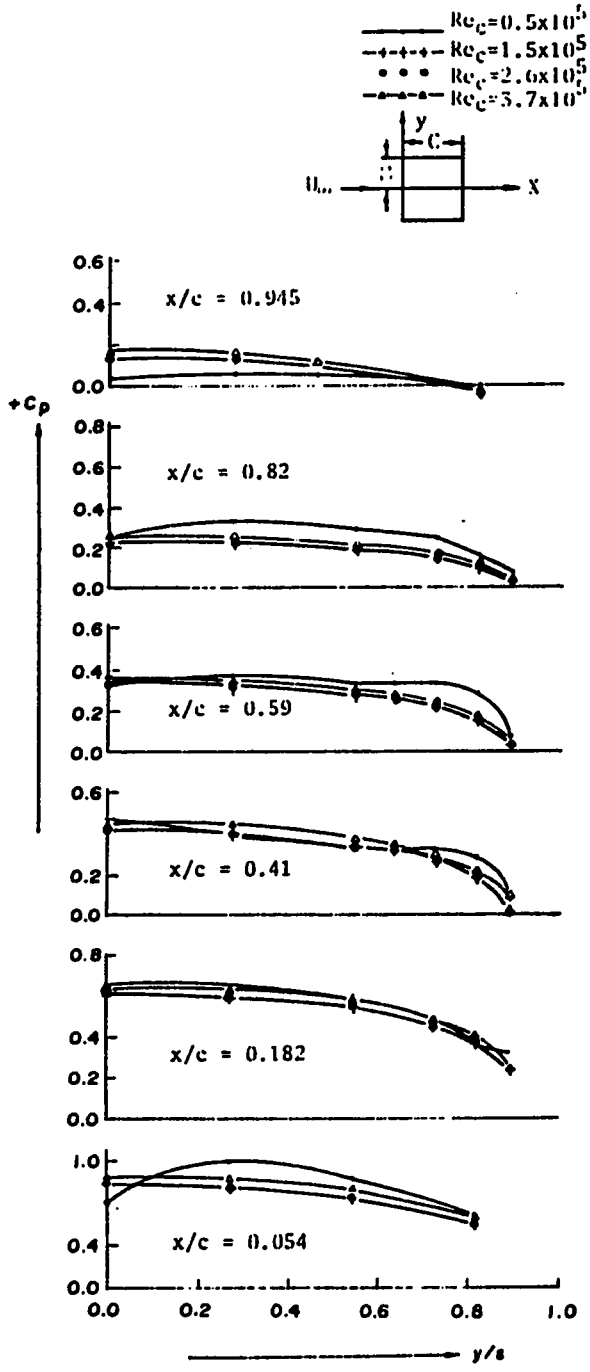

Fig. 3.19. Spanwise pressure distribution, α = 28°. Pressure side.

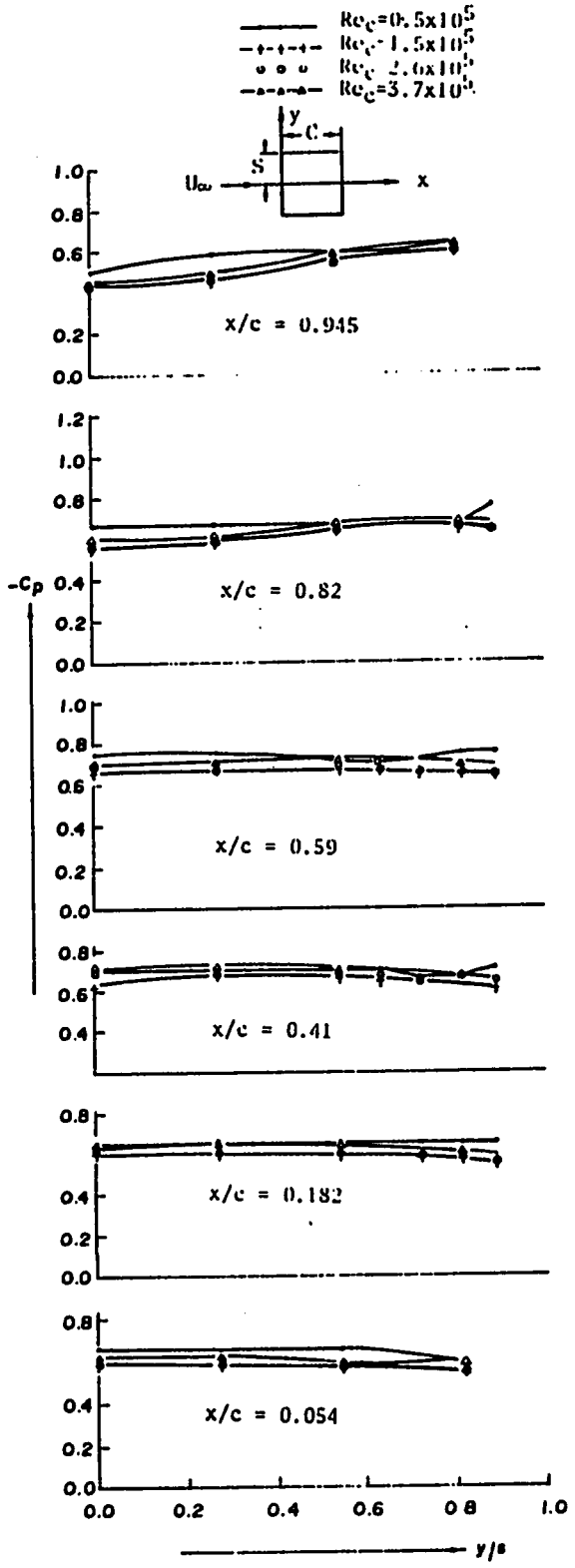

Fig. 3.20. Spanwise pressure distribution, $\alpha = 32°$. Suction side.

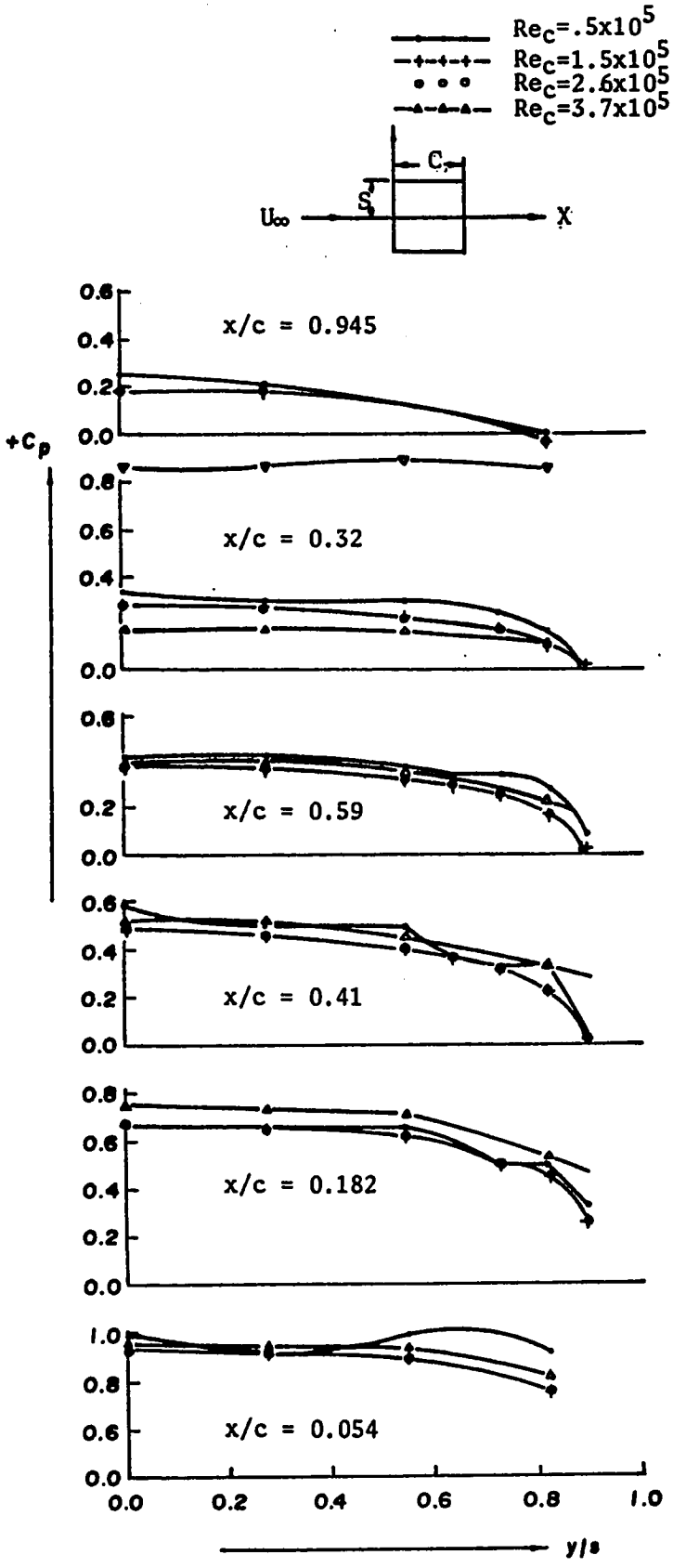

Fig.3.21. Spanwise pressure distribution, $\alpha=32^{o}$. Pressure side.

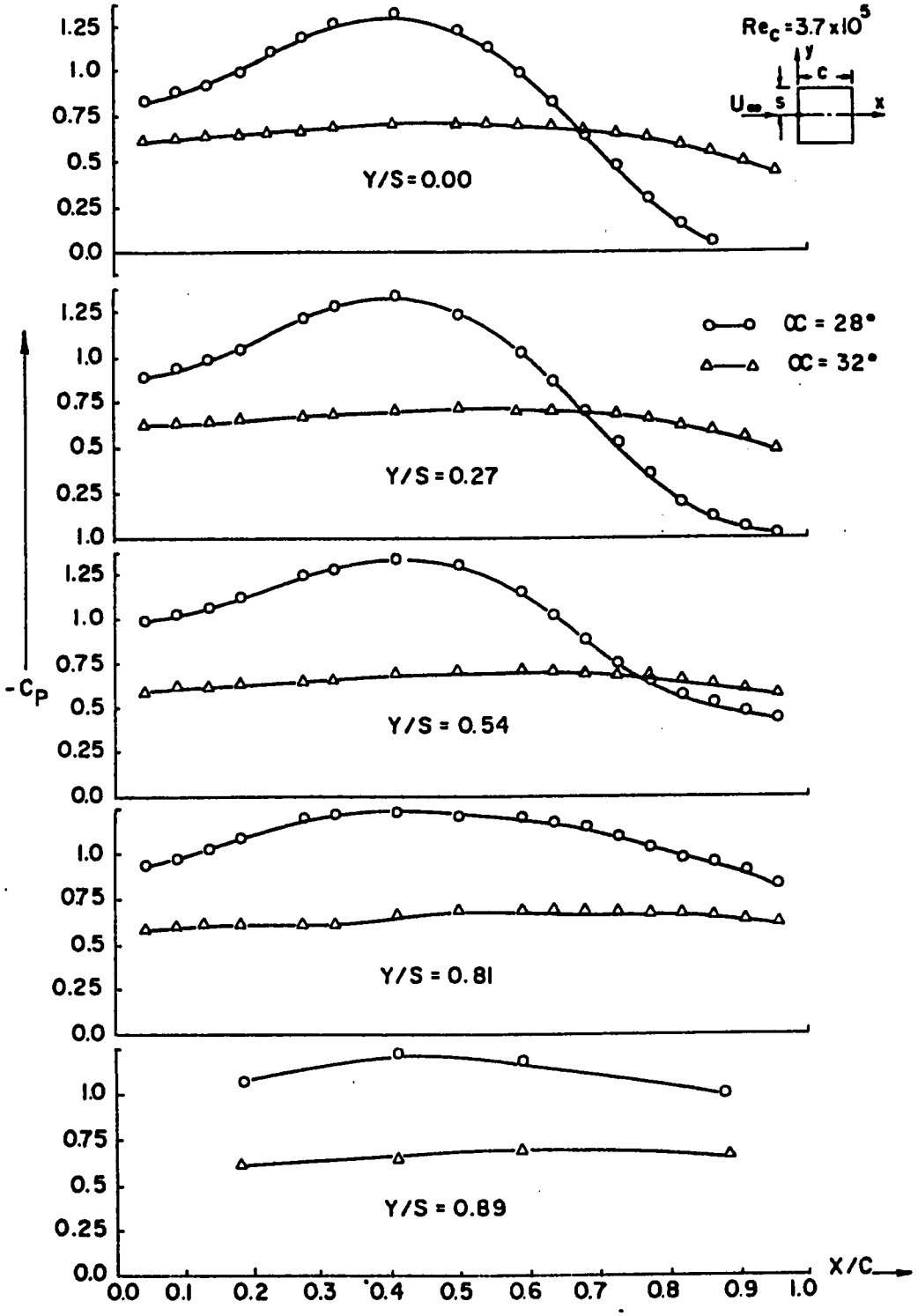

Fig.3.22. Chordwise Pressure Distribution on Suction Side of Square Plate.

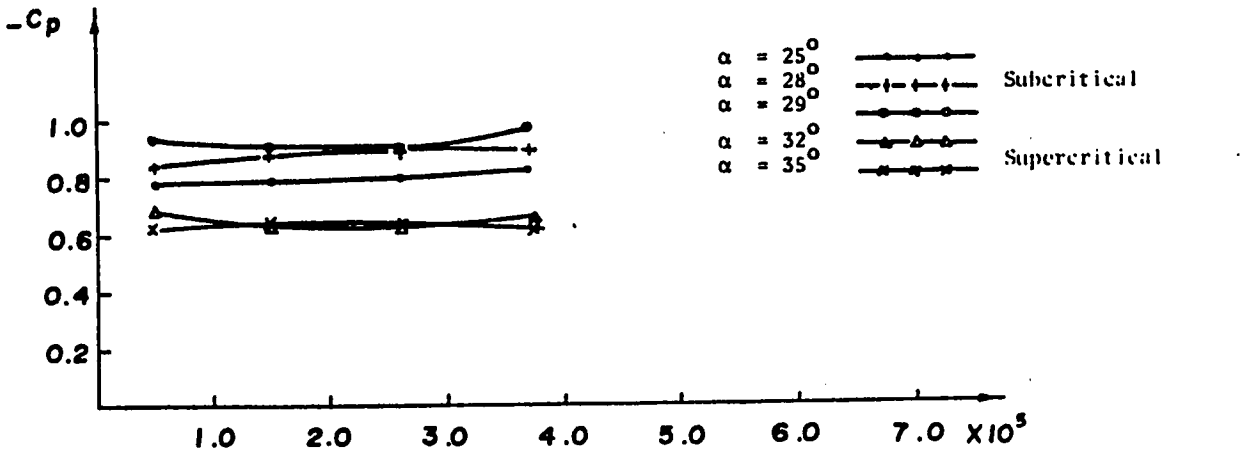

Fig. 3.23. Average mean pressure coefficient vs. Reynolds number, suction side.

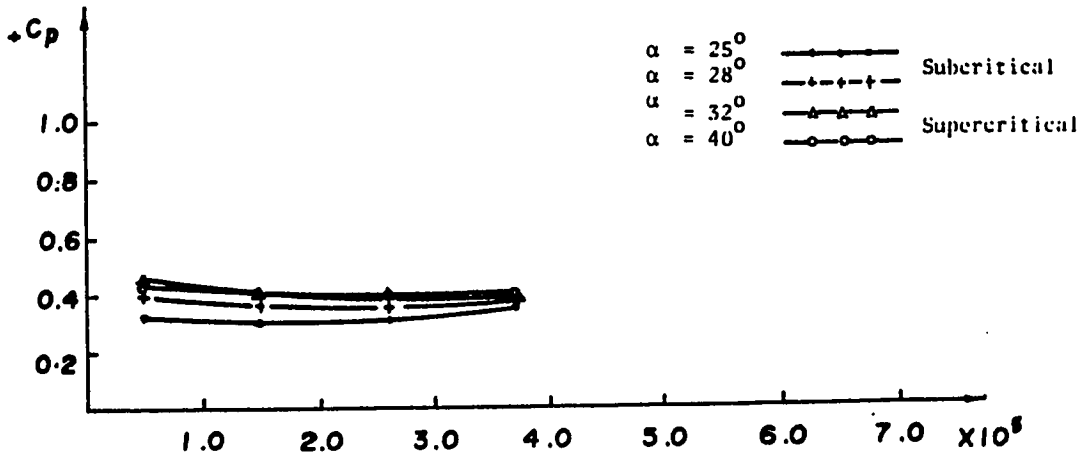

Fig. 3.24. Average mean pressure coefficient vs. Reynolds number, pressure side.

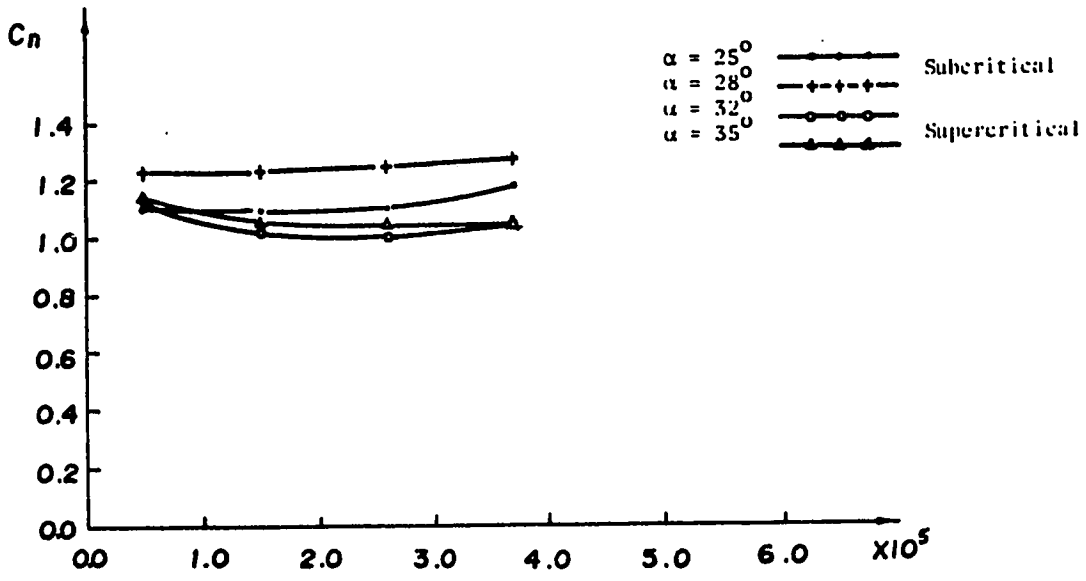

Fig. 3.25. Normal force coefficient vs. Reynolds number for square flat plate.

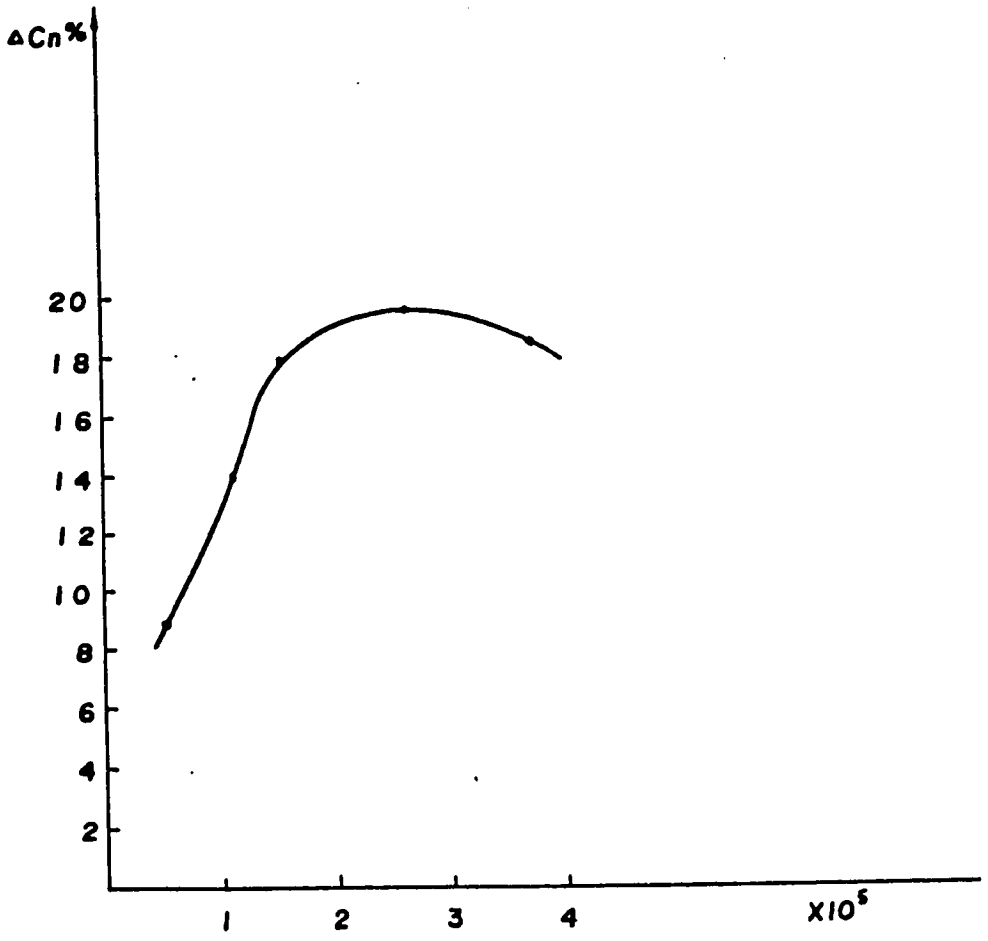

Fig. 3.26. Percentage drop in normal force vs. Reynolds number for square flat plate.

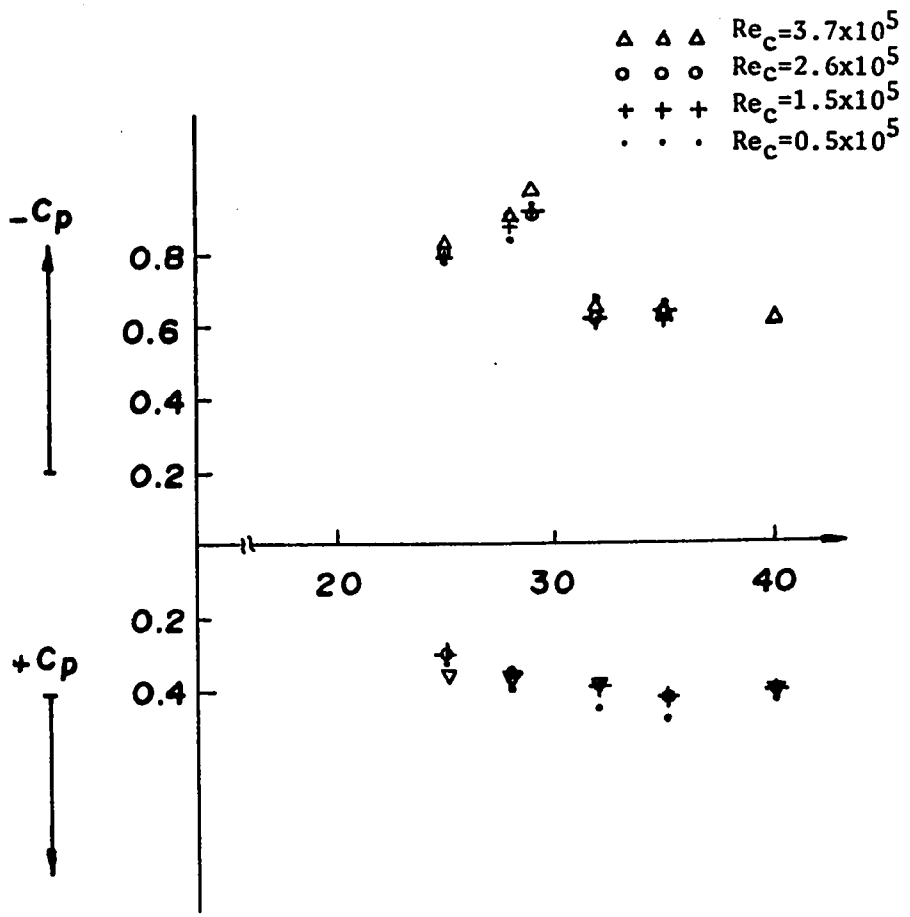

Fig.3.27. Average mean pressure coefficient vs. angle of attack for square flat plate.

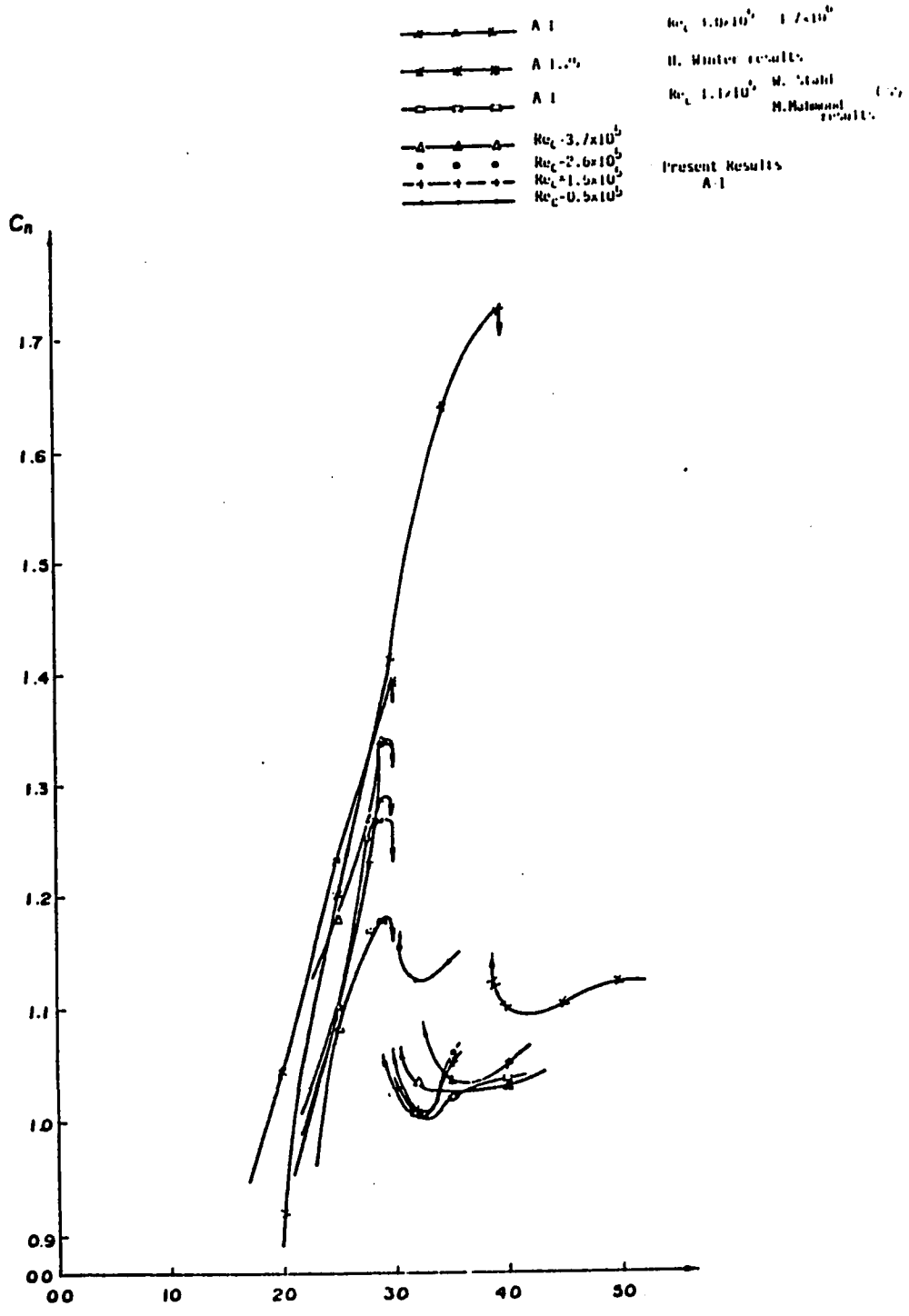

Fig. 3.28. Normal force coefficient vs. angle of attack for rectangular plates.

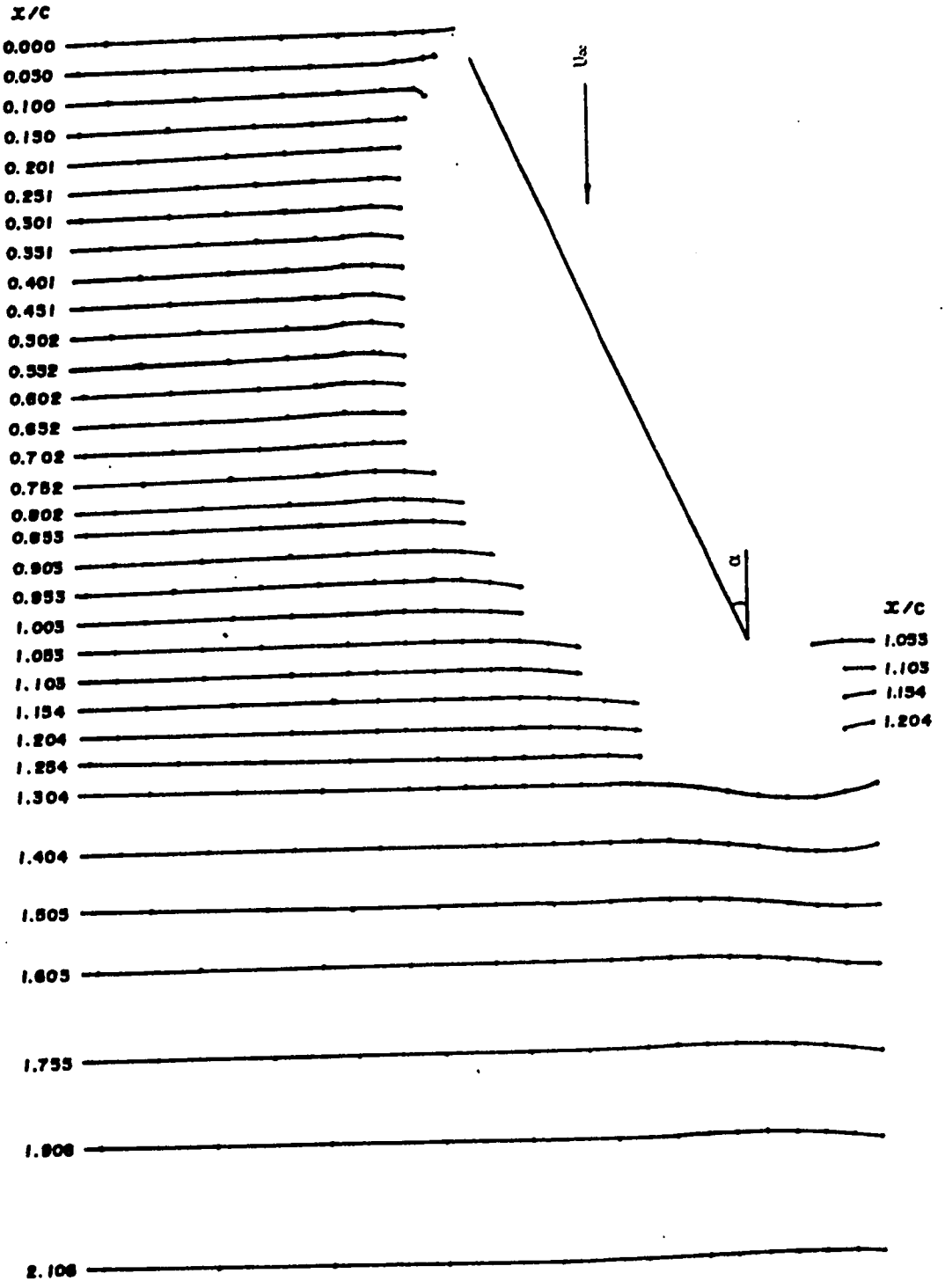

Fig. 3.29. Mean velocity profiles at the central plane of square flat plate, $Re_C = 0.5 \times 10^5$, $\alpha = 25°$.

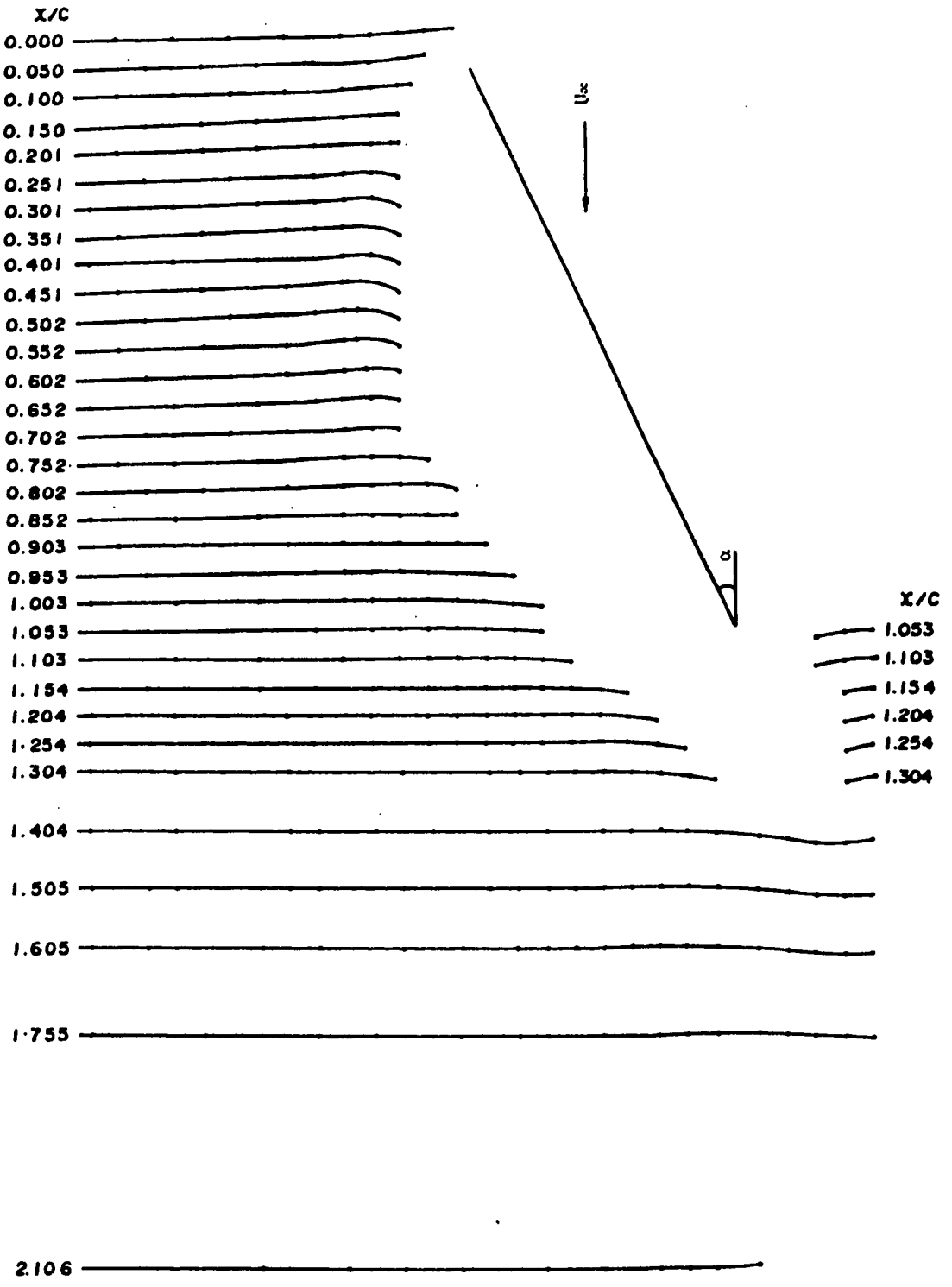

Fig. 3.30. Mean velocity profiles at the central plane of square flat plate, $Re_c = 1.5 \times 10^5$, $\alpha = 25°$.

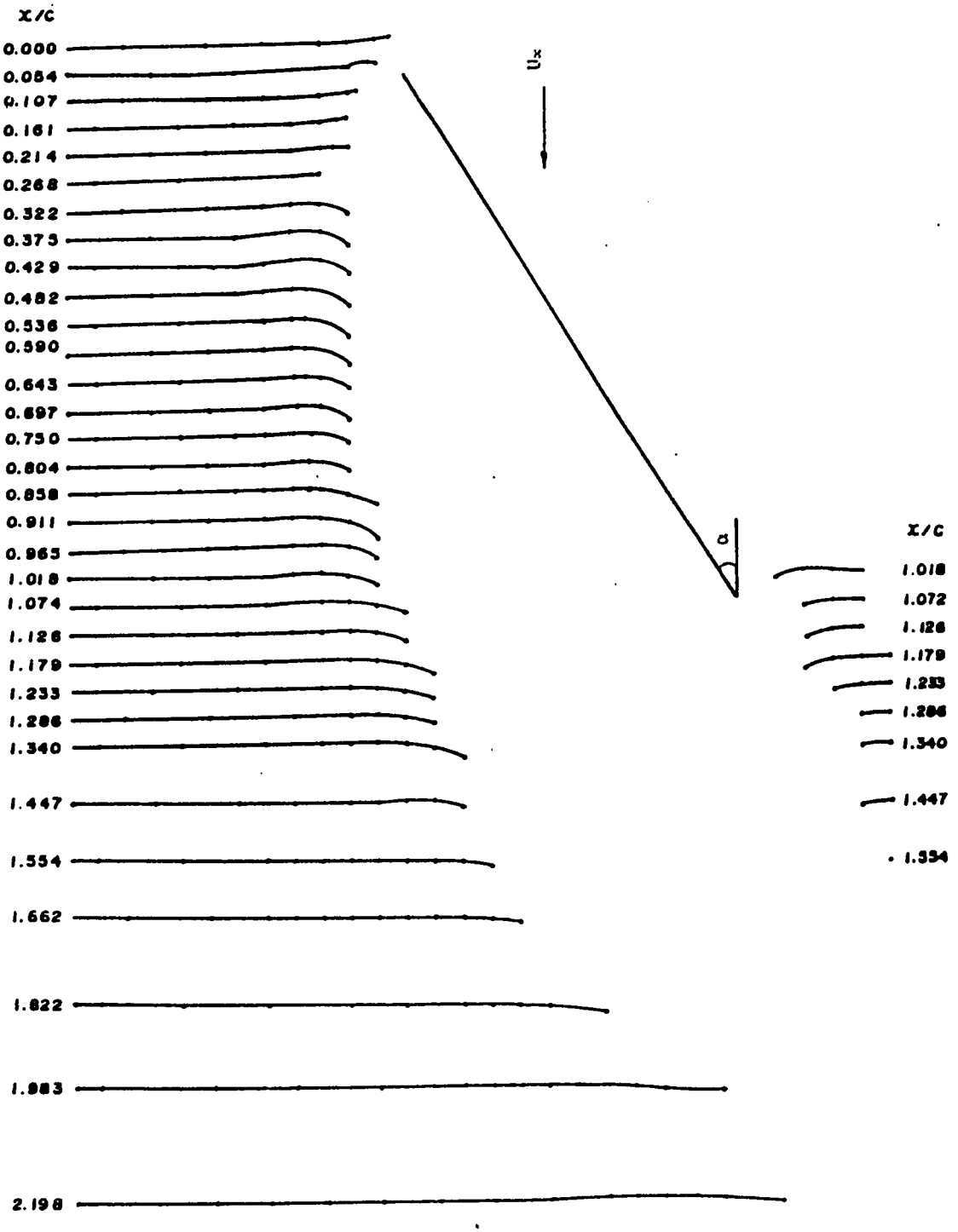

Fig. 3.31. Mean velocity profiles at the central plane of square flat plate, $Re_c = 0.5 \times 10^5$, $\alpha = 32°$.

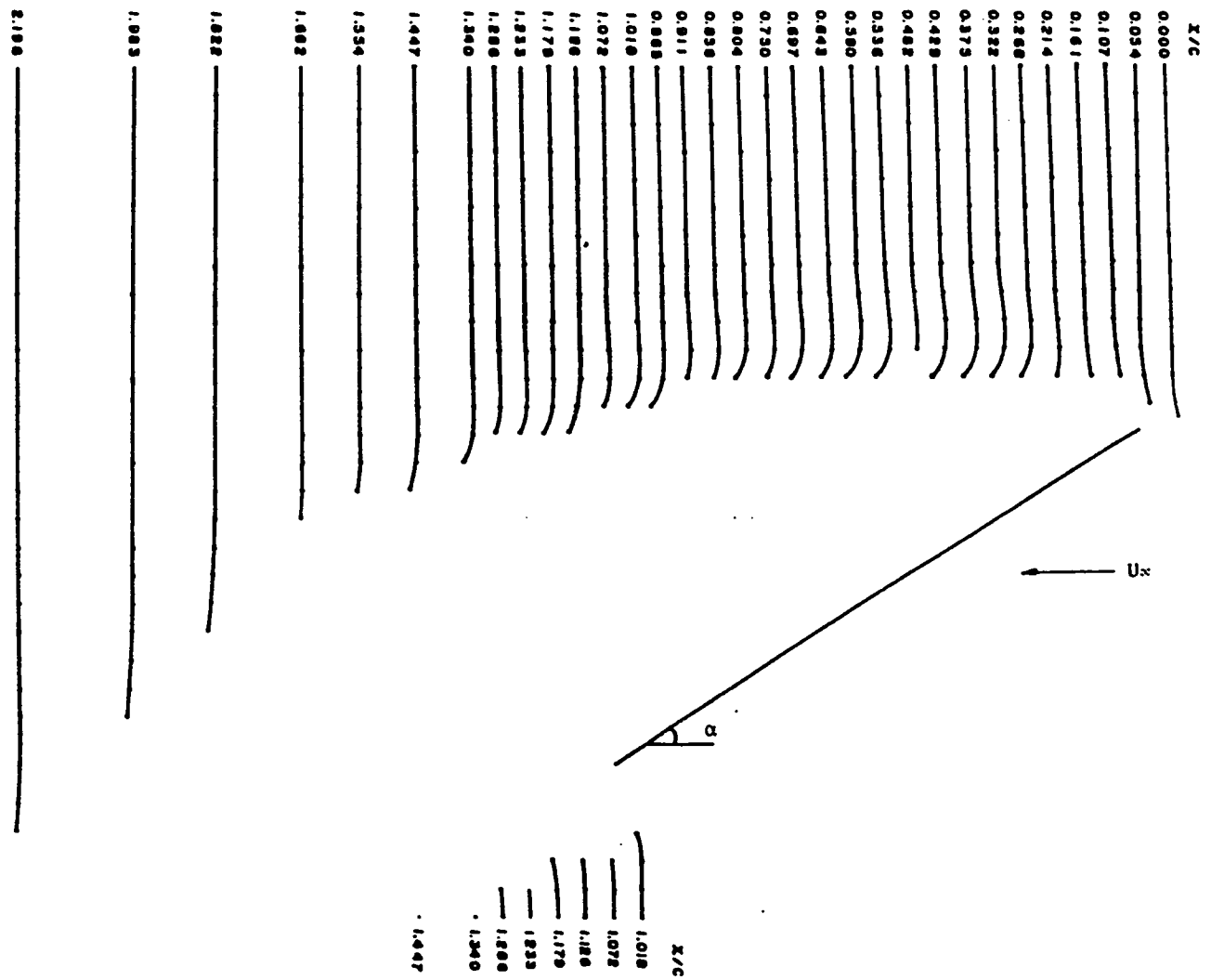

Fig. 3.32. Mean velocity profiles at the central plane of square flat plate. $Re_c = 1.5 \times 10^5$, $\alpha = 32°$.

RMS $Re_c=1.5\times10^5$	RMS $Re_c=0.5\times10^5$
Millivolts	
188	234
249	665
295	546
552	570
496	600
318	524
515	528
384	787
625	661
420	1140
491	1140
542	1200
475	927
561	867
465	707
375	575
634	853
445	590
324	478
313	620
190	382
214	400
224	305
178	380
167	245
215	333
315	474
332	524
271	441
181	332
204	332

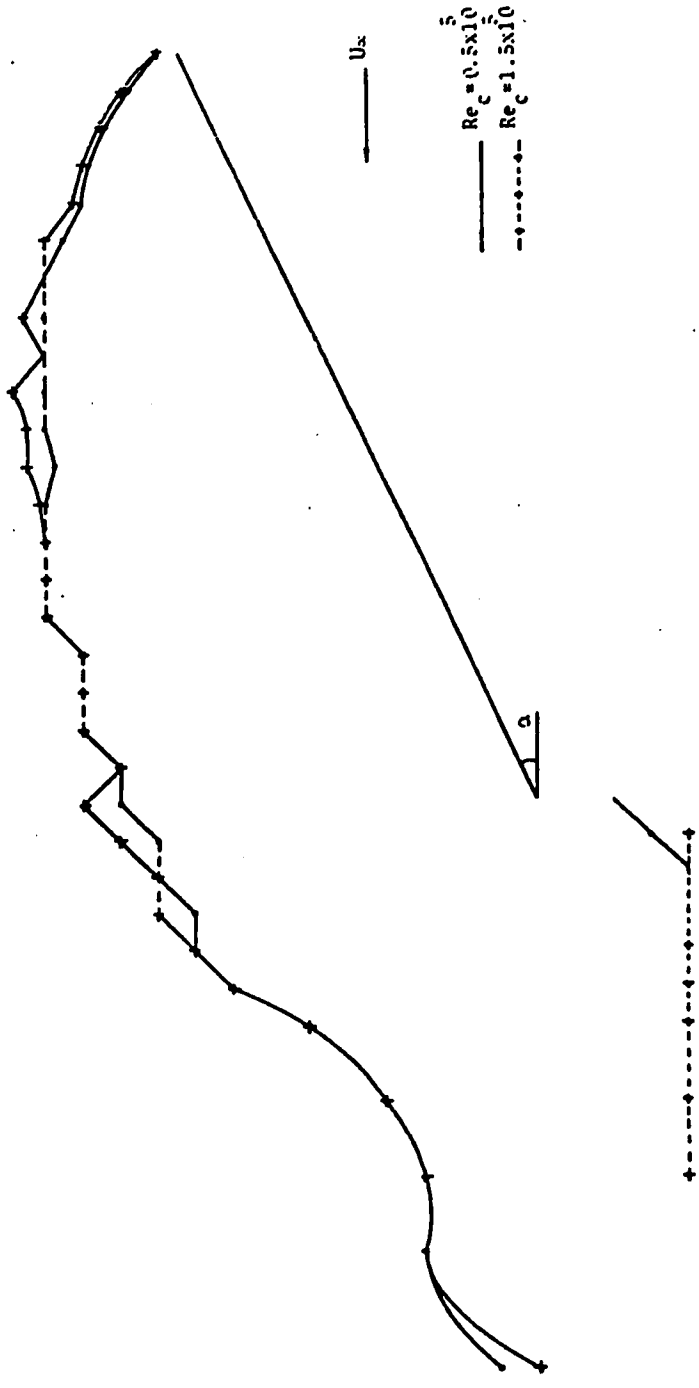

Fig. 3.33. Mean wake boundary at the central plane of square flat plate, α = 25°.

RMS $Re_c=1.5\times10^5$	RMS $Re_c=0.5\times10^5$
Millivolts	
19.1	45.6
46.5	183
85	595
346	730
29.5	371
83	337
132	620
167	630
189	650
322	420
302	480
367	456
303	342
301	297
253	420
367	382
194	312
196	504
176	421
140	310
275	405
223	335
185	275
148	425
306	342
193	264
115	342
282	395
144	246
144	168
295	265
528	652

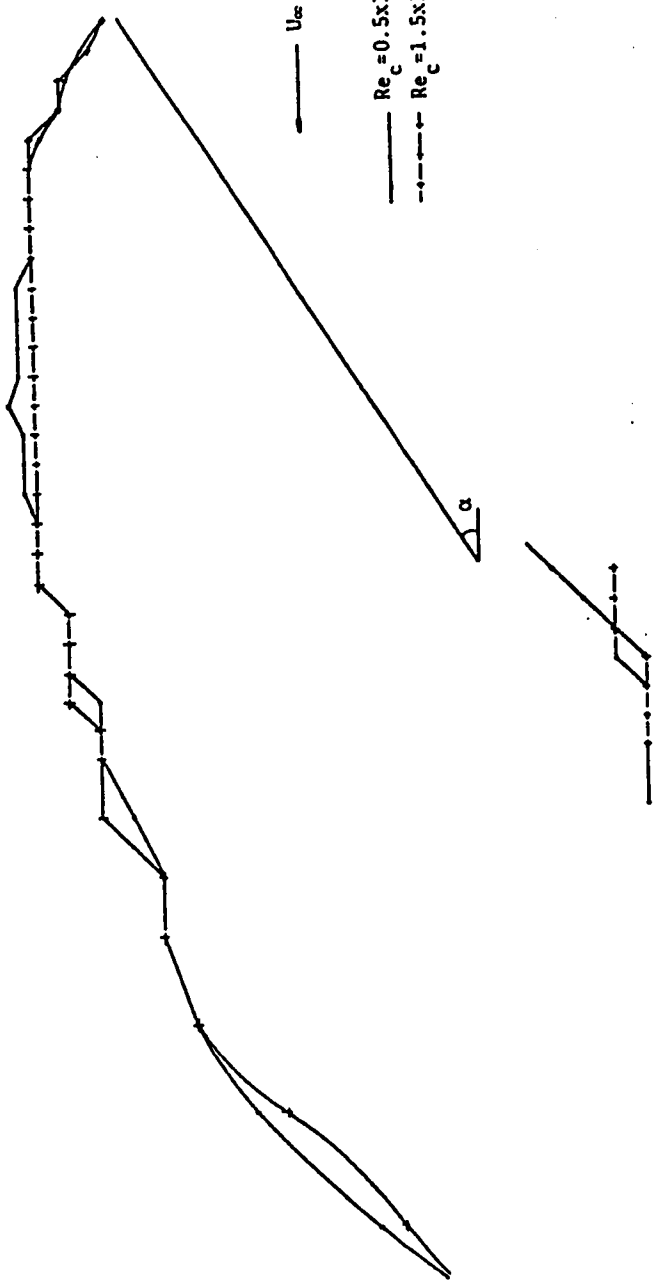

Fig. 3.34. Mean wake boundary at the central plane of square flat plate, α = 32°.

U_∞ m/s	Re_c
3.20	0.5×10^5
10.12	1.5×10^5
17.40	2.6×10^5
24.00	3.7×10^5

Table 2.2.1

Re_c	α	$-\overline{C}_p$	$+\overline{C}_p$	C_n
0.5×10^5	25^o	0.777	0.326	1.103
	28^o	0.837	0.391	1.228
	29^o	0.929		
	32^o	0.676	0.447	1.123
	35^o	0.658	0.478	1.136
	40^o		0.429	
1.5×10^5	25^o	0.789	0.304	1.093
	28^o	0.877	0.351	1.228
	29^o	0.914		
	32^o	0.616	0.392	1.008
	35^o	0.637	0.413	1.05
	40^o		0.402	
2.6×10^5	25^o	0.796	0.305	1.101
	28^o	0.897	0.352	1.249
	29^o	0.904		
	32^o	0.617	0.389	1.006
	35^o	0.638	0.419	1.057
	40^o		0.40	
3.7×10^5	25^o	0.826	0.35	1.176
	28^o	0.896	0.368	1.264
	29^o	0.966		
	32^o	0.65	0.382	1.032
	35^o	0.623		
	40^o	0.613	0.399	1.03

Table 3.3.1

Re_c	0.5×10^5	1.1×10^5	1.5×10^5	2.6×10^5	3.7×10^5
ΔC_n%	8 .6	13.9*	17.9	19.5	18.4

Table 3.3.2

* This value is taken from (22)